

Active Spaces and Non-Orthogonal Configuration Interaction Approaches for Investigating Molecules on Metal Surfaces

Junhan Chen,[†] Wenjie Dou,^{‡,¶} and Joseph Subotnik^{*,†}

[†]*Department of Chemistry, University of Pennsylvania, Philadelphia, Pennsylvania 19104, USA*

[‡]*School of Science, Westlake University, Hangzhou, Zhejiang 310024, China*

[¶]*Institute of Natural Sciences, Westlake Institute for Advanced Study, Hangzhou, Zhejiang 310024, China*

E-mail: subotnik@sas.upenn.edu

Phone: +1 (215) 746-7078

Abstract

We test a set of multiconfigurational wavefunction approaches for calculating the ground state electron population for a two-site Anderson model representing a molecule on a metal surface. In particular, we compare (*i*) a Hartree Fock like wavefunction where frontier orbitals are allowed to be nonorthogonal versus (*ii*) a fully non-orthogonal configuration interaction wavefunction based on constrained Hartree-Fock states. We test both the strong and weak metal-molecule hybridization (Γ) limits as well as the strong and weak electron-electron repulsion (U) limits. We obtain accurate results as compared with exact numerical renormalization group (NRG) theory, recovering charge transfer states where appropriate. The current framework should open a path to run molecular non-adiabatic dynamics on metal surfaces.

I Introduction

Solving embedding problem has attracted a great deal of attention in recent years¹⁻¹¹ as chemists look to exploring interesting interfacial phenomena, e.g., molecular resonance effects on metal surfaces,¹² electron-coupled adsorption¹³ and electron-coupled vibration.^{14,15} Embedding theory provides an attractive strategy to describe the electronic structure of extended systems (including interfacial systems) which can be impractical for traditional high accuracy quantum mechanics methods, e.g. coupled-cluster singles, doubles and full triples (CCSDT),¹⁶ second-order perturbation with complete active space (CASPT2)^{17,18} and multireference configuration interaction (MRCI)¹⁹ or full configuration interaction (FCI).^{20,21}

Historically, some of the earliest embedding calculations have addressed the Anderson Impurity model²² (or the more general Hubbard model). By now, this model has been analyzed by a variety of exact impurity solvers including the numerical renormalization group (NRG),²³ exact diagonalization (ED)²⁴ and quantum monte carlo (QMC).²⁵ These benchmark studies have then been very useful as far as benchmarking other, not exact but powerful, embedding methods, including dynamical mean-field theory (DMFT)²⁶ and density matrix embedding theory (DMET).⁵ To date, however, many of these powerful methods still have not been applied to study the problem of embedding realistic molecules on a realistic metal surface where there are many two-electron matrix elements. For such a mundane task, constrained DFT (CDFT) still remains the most practical approach, and the method has been applied successfully to some extent.²⁷⁻³⁰ That being said, CDFT results can also be unreliable in some cases, e.g. strong molecule-metal coupling (i.e. strong hybridization)¹² and fractional charge transfer.³¹ Nonadiabatic dynamics remains just out of reach for many realistic potentials.

With this background in mind, the goal of this paper is to introduce an new electronic structure method designed specifically to address a molecule on a metal surface. Importantly, when the electron-electron repulsion energy on the impurity becomes large compared with the impurity-metal coupling (i.e. in the weak metal-molecule coupling limit), the true

wavefunction will exhibit strong multireference character. In such a case, we must be able to capture the open-shell singlet character for an electron on or off the impurity; a single determinant wavefunction will not be a good reference in such a case. At the same time, of course, the correct wavefunction *will* exhibit simple single-reference character in the limit of strong metal-molecule coupling, and a good solver must reduce to the RHF solution in such a case. With these two limits in mind, below we explore a very basic approach whereby the frontier orbitals are modulated so that the total wavefunction will indeed contain open-shell character in the weak coupling limit and closed-shell character in the strong coupling limit. We call the resulting ansatz a closed-or-open shell Hartree Fock (COOS-HF) wavefunction.

In what follows, our specific goal will be to derive the necessary equations for solving for the COOS-HF equations just described, to apply this method to the Anderson Impurity model, and to compare our results to a constrained Hartree-Fock/Nonorthogonal configuration interaction (CHF/NOCI) formalism. We will show that surprisingly accurate results can be found with only a few variables to be optimized. We note that these results follow our previous work in embedding using configuration interaction spaces,^{32,33} but we emphasize that the present approach does not require diagonalizing a massive matrix of any kind.

An outline of this manuscript is as follows. In Sec. II, we introduce the COOS-HF formalism and we review the basic elements of a standard CHF/NOCI approach; we also include a brief comparison between COOS-HF and CASSCF(2,2) in subsection IIC.1. In Sec. III, we show results for the ground state population and energy, from which one can evaluate the accuracy of our approach. In Sec. IV, we discuss spin-contamination and show that the present approach is free of any contamination. Furthermore, we contemplate different variations of the COOS-HF ansatz that one can imagine implementing (e.g., [partially optimized] poCOOS-HF vs [fully optimized] foCOOS-HF) and we place our results in the context of a CASSCF(2,2) formalism. We conclude in Sec. V.

II Theory

A The Model: Two-Site Anderson Impurity Model

For this paper, our model of choice will be the two-site Anderson impurity model (AIM).

Within a second quantized representation, the Hamiltonian can be written as:

$$\begin{aligned}
 \hat{H} &= \hat{H}_{one} + \hat{\Pi} \\
 \hat{H}_{one} &= \epsilon_{d_1} \sum_{\sigma} d_{1\sigma}^{\dagger} d_{1\sigma} + \epsilon_{d_2} \sum_{\sigma} d_{2\sigma}^{\dagger} d_{2\sigma} + t_d \sum_{\sigma} (d_{1\sigma}^{\dagger} d_{2\sigma} + d_{2\sigma}^{\dagger} d_{1\sigma}) \\
 &\quad + \sum_{k\sigma} \epsilon_{k\sigma} c_{k\sigma}^{\dagger} c_{k\sigma} + \sum_{k\sigma} V_k (d_{1\sigma}^{\dagger} c_{k\sigma} + c_{k\sigma}^{\dagger} d_{1\sigma}) \\
 \hat{\Pi} &= U (d_{1\uparrow}^{\dagger} d_{1\uparrow} d_{1\downarrow}^{\dagger} d_{1\downarrow} + d_{2\uparrow}^{\dagger} d_{2\uparrow} d_{2\downarrow}^{\dagger} d_{2\downarrow})
 \end{aligned} \tag{1}$$

and the mean-field Fock operator (assuming spin restricted case) can be easily written as:

$$\hat{F} = \hat{H}_{one} + U \langle d_1^{\dagger} d_1 \rangle d_1^{\dagger} d_1 + U \langle d_2^{\dagger} d_2 \rangle d_2^{\dagger} d_2 \tag{2}$$

Here, $\{\hat{d}_1^{\dagger}, \hat{d}_2^{\dagger}\}$ refer to impurity atomic orbitals, the operators \hat{c}_k^{\dagger} refer to bath (metal surface) atomic orbitals, and σ refers to an electron spin. $\epsilon_{d_1}, \epsilon_{d_2}$ and ϵ_k are one-electron ionization energies for the impurities and bath. t_d is the hopping parameter between site 1 and site 2, U represents the on-site coulomb repulsion for the impurity. V_k represents the hybridization between impurity site 1 and the metal bath, and as in the wide band approximation, is characterized by:

$$\Gamma = \Gamma(\epsilon) = 2\pi \sum_k |V_k|^2 \delta(\epsilon - \epsilon_k), \tag{3}$$

where Γ is assumed to be constant through the whole energy spectrum ϵ .

The Hamiltonian in Eq. 1 characterizes many different physical processes because, in certain parameter regimes, one can identify states with effectively open shell singlet character

within the set of impurity orbitals; in other regimes, one can identify charge transfer between impurity and metal; and of course these two phenomena cannot be fully disentangled for all parameter regimes, highlighting a more realistic version of electron-electron correlation than is found for a single-site Anderson Holstein Hamiltonian.

We will now address the two wavefunction approaches that we wish to compare as far as assessing the ground-state electronic structure for the system plus bath: a constrained Hartree Fock configuration interaction approach versus a closed-or-open-shell frontier orbital wavefunction approach.

B Method 1: Constrained Hartree-Fock Based Nonorthogonal Configuration Interaction (CHF/NOCI)

B.1 Constrained HF states

Following Ref.,³⁴ a general constraint to the density can often be written as,

$$\sum_{\sigma} \int w_c^{\sigma}(\mathbf{r}) \rho^{\sigma}(\mathbf{r}) d\mathbf{r} = N_c \quad (4)$$

where $w_c(\mathbf{r})$ acts as a weight function that defines the constrained property, σ represents the electron spin, $\rho(\mathbf{r})$ represents the charge density and N_c represents the total number of constrained charge (or electrons). By adding one Lagrange multiplier, V_c , one can optimize a general functional of the density $E[\rho]$ with a prescribed constraint by looking for extrema of the following function:

$$W[\rho, V_c] = E[\rho] + V_c \left(\sum_{\sigma} \int w_c^{\sigma}(\mathbf{r}) \rho^{\sigma}(\mathbf{r}) d\mathbf{r} - N_c \right) \quad (5)$$

Within constrained density functional theory,³⁴ one looks to minimize the energy functional with the constraint that orbitals are normalized, and one then arrives at the standard con-

strained DFT equations:

$$\left(-\frac{1}{2}\nabla^2 + v_n(\mathbf{r}) + \int \frac{\rho(\mathbf{r}')}{|\mathbf{r} - \mathbf{r}'|} d\mathbf{r}' + v_{xc\sigma}(\mathbf{r}) + V_c w_c^\sigma(\mathbf{r})\right) \psi_{i\sigma} = \epsilon_{i\sigma} \psi_{i\sigma} \quad (6)$$

This language (based on continuous real space or plane wave basis sets) can easily be extended to the realm of discretized site basis sets as appropriate for a generalized Anderson model under a restricted Hartree-Fock (RHF) framework. The relevant density constraint (defining the number of electrons on the impurity) becomes

$$\text{Tr}(\hat{\rho}\hat{w}_c) = N_c \quad (7)$$

where the density matrix $\hat{\rho}$ and the weight matrix \hat{w}_c are defined as:

$$\hat{\rho} = \sum_{i \in occ} |\psi_i\rangle\langle\psi_i| \quad (8)$$

$$\hat{w}_c = \sum_{\mu \in impurity} w_\mu |d_\mu\rangle\langle d_\mu| \quad (9)$$

Here, the set $\{|\psi_i\rangle\}$ are the eigenvectors of the Hartree-Fock equation and we set all site weights as $w_\mu = 1$. Specifically speaking, the weight matrix for two-site Anderson model will be:

$$\hat{w}_c = |d_1\rangle\langle d_1| + |d_2\rangle\langle d_2| \quad (10)$$

We will explore all possible integer values for the constrained number of integer electrons on the two impurity sites:

$$N_c \in \{0e, 1e, 2e, 3e, 4e\} \quad (11)$$

The final constrained Hartree-Fock equation can be written as

$$\left(\hat{F} + V_c \hat{w}_c\right) \psi_i = \epsilon_i \psi_i, \quad (12)$$

where the fock matrix \hat{F} is defined in Eq. 2. Note that even though N_c is not explicitly included in Eq. 12, a value of N_c is required to find the optimized Lagrange multiplier, V_c .

Here we use the first derivative and second derivative³⁴ of $W(V_c)$ (assuming restricted orbitals) in Eq. 5:

$$\frac{dW}{dV_c} = \sum_{\sigma} \int w_c^{\sigma}(\mathbf{r})\rho^{\sigma}(\mathbf{r})d\mathbf{r} - N_c = 2 \langle d_1 | \hat{\rho} | d_1 \rangle + 2 \langle d_2 | \hat{\rho} | d_2 \rangle - N_c \quad (13)$$

$$\frac{d^2W}{dV_c^2} = 2 \sum_{\sigma} \sum_i^{N_{\sigma}} \sum_{a>N_{\sigma}} \frac{|\langle \psi_{i\sigma} | w_c^{\sigma} | \psi_{a\sigma} \rangle|^2}{\epsilon_{i\sigma} - \epsilon_{a\sigma}} = 4 \sum_{i \in occ} \sum_{a \in vir} \frac{|\langle \psi_i | w_c | \psi_a \rangle|^2}{\epsilon_i - \epsilon_a} \quad (14)$$

Here $\hat{\rho}$ is the density matrix operator defined in Eq. 8, d_1 and d_2 represent two impurity sites, w_c is the weight matrix defined in Eq. 10, $\{\psi_i\}$ or $\{\psi_a\}$ and ϵ_i or ϵ_a are eigenvectors and eigenvalues of Eq. 12, respectively. As discussed in Ref.³⁴, Eq. 14 is derived from simple first-order perturbation theory of the Kohn-Sham equations. An algorithm to determine the constrained Hartree-Fock solution can be summarised as follows:

1. Choose the desired value of N_c in Eq. 11;
2. Guess a Lagrange multiplier, e.g. $V_c = 0$;
3. Guess an impurity population $\langle d_1^{\dagger} d_1 \rangle = \langle d_2^{\dagger} d_2 \rangle = \frac{N_c}{4}$;
4. Construct the Fock matrix using Eq. 2;
5. Solve Eq. 12 self-consistently and obtain eigenvectors $\{\psi\}$ and eigenvalues $\{\epsilon\}$;
6. Calculate a new impurity population $\langle d_1^{\dagger} d_1 \rangle$ and $\langle d_2^{\dagger} d_2 \rangle$;
7. Take a Newton step to calculate a new V_c by Eqs. 13-14;
8. Repeat Step 4-7 until V_c converges.

B.2 Non-Orthogonal Configuration Interaction

The total number of electrons on the two impurity sites is required to be an integer between 0 and 4. Therefore, one naturally finds five diabatic constrained Hartree-Fock (CHF) states for our model problem: $|\Phi_{4e}\rangle, |\Phi_{3e}\rangle, |\Phi_{2e}\rangle, |\Phi_{1e}\rangle, |\Phi_{0e}\rangle$, respectively. Since these configurations are not orthogonal to each other, a configuration interaction Hamiltonian can be constructed as (see Appendix VIA for a detailed derivation of the necessary matrix elements),

$$H^{CHF/NOCI} = \begin{bmatrix} \langle \Phi_{4e} | H | \Phi_{4e} \rangle & \langle \Phi_{4e} | H | \Phi_{3e} \rangle & \langle \Phi_{4e} | H | \Phi_{2e} \rangle & \langle \Phi_{4e} | H | \Phi_{1e} \rangle & \langle \Phi_{4e} | H | \Phi_{0e} \rangle \\ \langle \Phi_{3e} | H | \Phi_{4e} \rangle & \langle \Phi_{3e} | H | \Phi_{3e} \rangle & \langle \Phi_{3e} | H | \Phi_{2e} \rangle & \langle \Phi_{3e} | H | \Phi_{1e} \rangle & \langle \Phi_{3e} | H | \Phi_{0e} \rangle \\ \langle \Phi_{2e} | H | \Phi_{4e} \rangle & \langle \Phi_{2e} | H | \Phi_{3e} \rangle & \langle \Phi_{2e} | H | \Phi_{2e} \rangle & \langle \Phi_{2e} | H | \Phi_{1e} \rangle & \langle \Phi_{2e} | H | \Phi_{0e} \rangle \\ \langle \Phi_{1e} | H | \Phi_{4e} \rangle & \langle \Phi_{1e} | H | \Phi_{3e} \rangle & \langle \Phi_{1e} | H | \Phi_{2e} \rangle & \langle \Phi_{1e} | H | \Phi_{1e} \rangle & \langle \Phi_{1e} | H | \Phi_{0e} \rangle \\ \langle \Phi_{0e} | H | \Phi_{4e} \rangle & \langle \Phi_{0e} | H | \Phi_{3e} \rangle & \langle \Phi_{0e} | H | \Phi_{2e} \rangle & \langle \Phi_{0e} | H | \Phi_{1e} \rangle & \langle \Phi_{0e} | H | \Phi_{0e} \rangle \end{bmatrix} \quad (15)$$

and the corresponding overlap S is expressed as:

$$S = \begin{bmatrix} 1 & \langle \Phi_{4e} | \Phi_{3e} \rangle & \langle \Phi_{4e} | \Phi_{2e} \rangle & \langle \Phi_{4e} | \Phi_{1e} \rangle & \langle \Phi_{4e} | \Phi_{0e} \rangle \\ \langle \Phi_{3e} | \Phi_{4e} \rangle & 1 & \langle \Phi_{3e} | \Phi_{2e} \rangle & \langle \Phi_{3e} | \Phi_{1e} \rangle & \langle \Phi_{3e} | \Phi_{0e} \rangle \\ \langle \Phi_{2e} | \Phi_{4e} \rangle & \langle \Phi_{2e} | \Phi_{3e} \rangle & 1 & \langle \Phi_{2e} | \Phi_{1e} \rangle & \langle \Phi_{2e} | \Phi_{0e} \rangle \\ \langle \Phi_{1e} | \Phi_{4e} \rangle & \langle \Phi_{1e} | \Phi_{3e} \rangle & \langle \Phi_{1e} | \Phi_{2e} \rangle & 1 & \langle \Phi_{1e} | \Phi_{0e} \rangle \\ \langle \Phi_{0e} | \Phi_{4e} \rangle & \langle \Phi_{0e} | \Phi_{3e} \rangle & \langle \Phi_{0e} | \Phi_{2e} \rangle & \langle \Phi_{0e} | \Phi_{1e} \rangle & 1 \end{bmatrix} \quad (16)$$

To transform the interaction Hamiltonian into an orthogonal configuration basis, a transformation matrix X will be introduced, which satisfies:

$$X^\dagger S X = I \quad (17)$$

In this paper, X is chosen as: $X = S^{-\frac{1}{2}}$. By diagonalizing the matrix $X^\dagger H^{CHF/NOCI} X$, one obtains five adiabatic constrained Hartree-Fock nonorthogonal configuration interaction (CHF/NOCI) states.

C Method 2: Closed or Open Shell Hartree-Fock (COOS-HF)

Having discussed a standard CHF/NOCI approach to charge transfer, let us now introduce an alternative multiconfigurational approach that is not based on a configuration interaction Hamiltonian but rather on a set of frontier (non-orthogonal) orbitals. Our approach is to consider a wavefunction of the following form:

$$|\Phi_{COOS-HF}\rangle = \frac{1}{\sqrt{N}}(|\Phi_{pq}\rangle + |\Phi_{qp}\rangle), \quad (18)$$

where N is the normalization factor:

$$N = 2(1 + \langle p|q\rangle^2), \quad (19)$$

\mathbf{p}, \mathbf{q} are two nonorthogonal orbitals and $|\Phi_{pq}\rangle, |\Phi_{qp}\rangle$ are the following two slater determinants for a $2n$ -electrons system:

$$|\Phi_{pq}\rangle = \begin{vmatrix} \psi_1(1) & \bar{\psi}_1(1) & \cdots & p(1) & \bar{q}(1) \\ \psi_1(2) & \bar{\psi}_1(2) & \cdots & p(2) & \bar{q}(2) \\ \vdots & \vdots & \ddots & \vdots & \vdots \\ \psi_1(2n) & \bar{\psi}_1(2n) & \cdots & p(2n) & \bar{q}(2n) \end{vmatrix} \quad (20)$$

$$|\Phi_{qp}\rangle = \begin{vmatrix} \psi_1(1) & \bar{\psi}_1(1) & \cdots & q(1) & \bar{p}(1) \\ \psi_1(2) & \bar{\psi}_1(2) & \cdots & q(2) & \bar{p}(2) \\ \vdots & \vdots & \ddots & \vdots & \vdots \\ \psi_1(2n) & \bar{\psi}_1(2n) & \cdots & q(2n) & \bar{p}(2n) \end{vmatrix} \quad (21)$$

For the moment, we make no stipulations about the character of the orbitals \mathbf{p} and \mathbf{q} ; they could be parallel or they could be orthogonal. And so, we refer to the wavefunction in Eq. 18 as a closed-or-open shell HF ansatz.

Two options are now possible as far optimizing such a COOS-HF wavefunction. First,

one could imagine optimizing all of the orbitals, $\{\psi_1, \psi_2, \dots, \mathbf{p}, \mathbf{q}\}$. We will call this approach a fully optimized COOS-HF (foCOOS-HF) ansatz.

The second approach is simpler and is based on a closed shell RHF reference state. In such a case, we can seek three nonorthogonal orbitals $\mathbf{o}, \mathbf{p}, \mathbf{q}$, so that a simplified partially optimized COOS-HF (poCOOS-HF) wavefunction can be written as:

$$|\Phi_{poCOOS-HF}\rangle = \frac{1}{\sqrt{N}}(|\Psi_{oo}^{p\bar{q}}\rangle + |\Psi_{oo}^{q\bar{p}}\rangle), \quad (22)$$

In Eq. 22, the choice of orbitals \mathbf{o}, \mathbf{p} , and \mathbf{q} is critical. For this wavefunction, we insist that orbital \mathbf{o} must be an occupied orbital, but we make no such assumption about orbitals \mathbf{p} and \mathbf{q} (our “active” orbitals) – even though p and q have been written for convenience in the superscript of the kets $|\Phi_{oo}^{p\bar{q}}\rangle$ and $|\Phi_{oo}^{q\bar{p}}\rangle$. More precisely, orbital \mathbf{p} need not be orthogonal to orbital \mathbf{o} or orbital \mathbf{q} . Thus, when we optimize Eq. 22 for orbitals \mathbf{o}, \mathbf{p} , and \mathbf{q} , we can indeed recover the starting RHF ansatz by picking $\mathbf{o}=\mathbf{p}=\mathbf{q}$.

In particular, we can parameterize the spatial components of \mathbf{o}, \mathbf{p} , and \mathbf{q} in the basis of RHF canonical occupied orbitals $\{o_i\}$ and virtual orbitals $\{v_a\}$:

$$\begin{aligned} |o\rangle &= \sum_i c_i |o_i\rangle \\ |p\rangle &= d_o |o\rangle + \sum_a d_a |v_a\rangle \\ |q\rangle &= \tilde{d}_o |o\rangle + \sum_b \tilde{d}_b |v_b\rangle \end{aligned} \quad (23)$$

Note that, if we define the core orbitals to be all of those occupied orbitals i orthogonal to orbital \mathbf{o} , the following identities also hold:

$$\langle i|o\rangle = 0 \quad (24)$$

$$\langle i|p\rangle = 0 \quad (25)$$

$$\langle i|q\rangle = 0 \quad (26)$$

and core orbitals \mathbf{i} together with orbital \mathbf{o} forms the RHF occupied space, i.e.:

$$\sum_i |i\rangle \langle i| + |o\rangle \langle o| = \sum_i |o_i\rangle \langle o_i| \quad (27)$$

C.1 COOS-HF as a subset of a CASSCF(2,2) calculation

The astute reader will notice that the COOS-HF wavefunction ansatz in Eq. 18 represents a singlet configuration without spin contamination and that the ansatz is clearly a subset of a CASSCF(2,2) ansatz by writing nonorthogonal orbitals \mathbf{p}, \mathbf{q} in the orthonormal basis \mathbf{a}, \mathbf{b} .

$$\begin{aligned} |p\rangle &= \cos \theta |a\rangle + \sin \theta |b\rangle \\ |q\rangle &= \cos \eta |a\rangle + \sin \eta |b\rangle \end{aligned} \quad (28)$$

Therefore, the wavefunction in Eq. 18 can be written as (for simplicity, core orbitals are ignored):

$$\frac{|p\bar{q}\rangle + |q\bar{p}\rangle}{\sqrt{N}} = \frac{1}{\sqrt{N}} \{2 \cos \theta \cos \eta |a\bar{a}\rangle + 2 \sin \theta \sin \eta |b\bar{b}\rangle + (\cos \theta \sin \eta + \cos \eta \sin \theta)(|a\bar{b}\rangle + |b\bar{a}\rangle)\} \quad (29)$$

This equation is clearly of the CASSCF(2,2) form (where the CI coefficients would normally be written as),

$$\alpha |a\bar{a}\rangle + \beta |b\bar{b}\rangle + \gamma(|a\bar{b}\rangle + |b\bar{a}\rangle) \quad (30)$$

if one makes the substitution:

$$\begin{aligned} \alpha &= \frac{2 \cos \theta \cos \eta}{\sqrt{N}} \\ \beta &= \frac{2 \sin \theta \sin \eta}{\sqrt{N}} \\ \gamma &= \frac{(\cos \theta \sin \eta + \cos \eta \sin \theta)}{\sqrt{N}} \end{aligned} \quad (31)$$

$$N = 2 * [1 + (\cos \theta \cos \eta + \sin \theta \sin \eta)^2]$$

A more complete discussion of this correspondence will be given in the discussion section.

C.2 Solving for the poCOOS-HF orbitals and energy

Let us now discuss how one can most easily solve for the poCOOS-HF orbitals. For the ansatz in Eq. 22, the expectation value for the total energy is:

$$\langle \Phi_{poCOOS-HF} | H | \Phi_{poCOOS-HF} \rangle = \frac{\langle \Psi_{oo}^{p\bar{q}} | H | \Psi_{oo}^{p\bar{q}} \rangle + \langle \Psi_{oo}^{p\bar{q}} | H | \Psi_{oo}^{q\bar{p}} \rangle}{1 + \langle p | q \rangle^2} \quad (32)$$

where

$$\begin{aligned} \langle \Psi_{oo}^{p\bar{q}} | H | \Psi_{oo}^{p\bar{q}} \rangle &= \langle \dots i \dots p \dots \bar{i} \dots \bar{q} | H | \dots i \dots p \dots \bar{i} \dots \bar{q} \rangle \\ &= 2h_{ii} + h_{pp} + h_{qq} + \left(\sum_i ii + pp | \sum_j jj + qq \right) \end{aligned} \quad (33)$$

$$\begin{aligned} \langle \Psi_{oo}^{p\bar{q}} | H | \Psi_{oo}^{q\bar{p}} \rangle &= \langle \dots i \dots p \dots \bar{i} \dots \bar{q} | H | \dots i \dots q \dots \bar{i} \dots \bar{p} \rangle \\ &= 2h_{ii} \langle p | q \rangle^2 + 2h_{pq} \langle p | q \rangle + \left(\sum_i ii \langle p | q \rangle + pq | \sum_j jj \langle p | q \rangle + pq \right) \end{aligned} \quad (34)$$

Furthermore, this expression can be simplified using E_{RHF} as a reference. Recall that the RHF energy is

$$E_{RHF} = 2h_{ii} + \sum_{ij} (ii|jj) + 2h_{oo} + 2 \sum_i (ii|oo) + (oo|oo), \quad (35)$$

If we then define Fock operators as:

$$\begin{aligned} f_{oo} &= h_{oo} + \sum_i (ii|oo) + (oo|oo) \\ f_{pp} &= h_{pp} + \sum_i (ii|pp) + (oo|pp) \\ f_{qq} &= h_{qq} + \sum_i (ii|qq) + (oo|qq) \\ f_{pq} &= h_{pq} + \sum_i (ii|pq) + (oo|pq) \end{aligned} \quad (36)$$

then the poCOOS-HF energy becomes:

$$\begin{aligned}
\langle \Phi_{poCOOS-HF} | H | \Phi_{poCOOS-HF} \rangle &= E_{RHF} - 2f_{oo} + (oo|oo) \\
&+ \frac{1}{1 + \langle p|q \rangle^2} [f_{pp} + f_{qq} + 2f_{pq} \langle p|q \rangle + 2(pp|qq)] \\
&- \frac{1}{1 + \langle p|q \rangle^2} [(oo|pp) + (oo|qq) + 2(oo|pq) \langle p|q \rangle]
\end{aligned} \tag{37}$$

Once the gradient is obtained (see AppendixVIB for a complete derivation of the analytical energy gradient), one can use a lagrange multiplier and a quasi-Newton method to minimize the objective function. To write the equations more succinctly, let us use the symbol x to represent a generic variable in the poCOOS-HF variable space in Eq. 23 (all of whose variables are denoted capital X):

$$X = \{\{c_i\}, d_o, \{d_a\}, \tilde{d}_o, \{\tilde{d}_b\}\} \tag{38}$$

The lagrangian operator can then be written as:

$$\min_{x \in X} \mathcal{L}(x) = E_{poCOOS-HF}(x) - \lambda_1 C_1(x) - \lambda_2 C_2(x) - \lambda_3 C_3(x), \tag{39}$$

where $\lambda_1, \lambda_2, \lambda_3$ are lagrange multipliers and the three constraints are:

$$\begin{aligned}
C_1(x) &= \sum_i c_i^2 - 1 \\
C_2(x) &= d_o^2 + \sum_a d_a^2 - 1 \\
C_3(x) &= \tilde{d}_o^2 + \sum_b \tilde{d}_b^2 - 1
\end{aligned} \tag{40}$$

Just as one would solve for an unconstrained objective function, we use a Newton iteration to solve for the present lagrangian (the so-called Newton-KKT equation):³⁵

$$\begin{bmatrix} \nabla_{xx}^2 \mathcal{L}_k & -\nabla C_1(x_k) & -\nabla C_2(x_k) & -\nabla C_3(x_k) \\ \nabla C_1^T(x_k) & 0 & 0 & 0 \\ \nabla C_2^T(x_k) & 0 & 0 & 0 \\ \nabla C_3^T(x_k) & 0 & 0 & 0 \end{bmatrix} \begin{bmatrix} p_k \\ \lambda_{1k} \\ \lambda_{2k} \\ \lambda_{3k} \end{bmatrix} = \begin{bmatrix} -\nabla E_{poCOOS-HF}(x_k) \\ -C_1(x_k) \\ -C_2(x_k) \\ -C_3(x_k) \end{bmatrix} \quad (41)$$

Here, p_k is the walking direction for x_k , i.e. $x_{k+1} = x_k + \alpha p_k$ and the step length α is obtained from a line search. To reduce the computational cost, the hessian $\nabla_{xx}^2 \mathcal{L}$ is also approximated and updated by a BFGS scheme. In practice, for the problems below and with a reasonable starting guess, we require roughly ten cycles (i.e. line searches).

III Results and discussion

In this paper, our goal is to compare the ground state properties (electron population and energy) as predicted by the methods (CHF/NOCI and poCOOS-HF) above and to assess their power for propagating adiabatic dynamics; in a future publication, we will address excited state properties (and e.g., we will benchmark against the ROKS method^{36,37}) so that we can assess running nonadiabatic dynamics. For the present case, because we focus on ground state theory, it is fairly straightforward to obtain exact benchmark energies using numerical renormalization group theory (NRG), which recovers only electron population (not total energy which would depend on the number of discrete orbitals in the bath). We will also benchmark our results against RHF and UHF.

Because molecules are very diverse and their properties can cover a multitude of chemisorption and physisorption regimes, we will test the algorithms above in three different onsite repulsion regimes: weak metal-molecule coupling $U = 10\Gamma$, intermediate coupling $U = 5\Gamma$ and strong coupling $U = \Gamma$. Fig. 1 plots the ground state spin-up electron population on

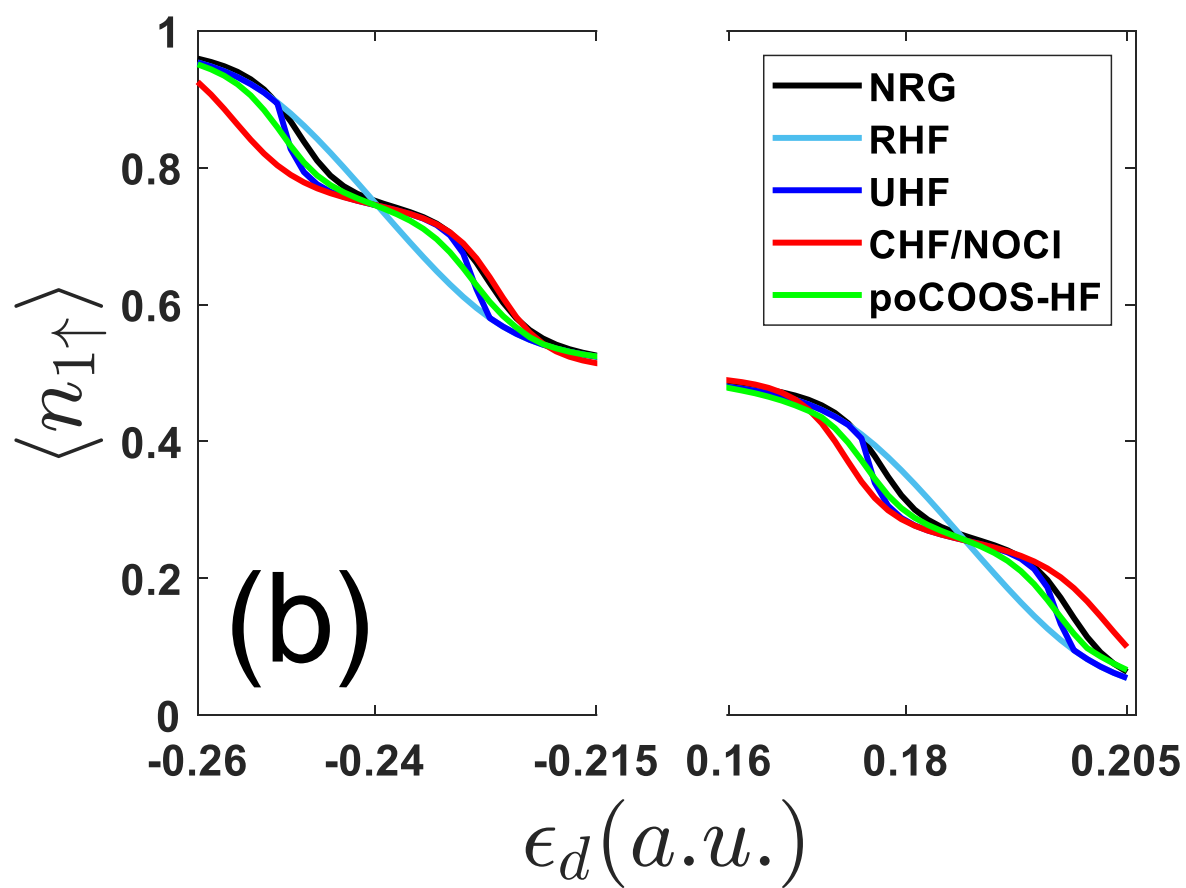
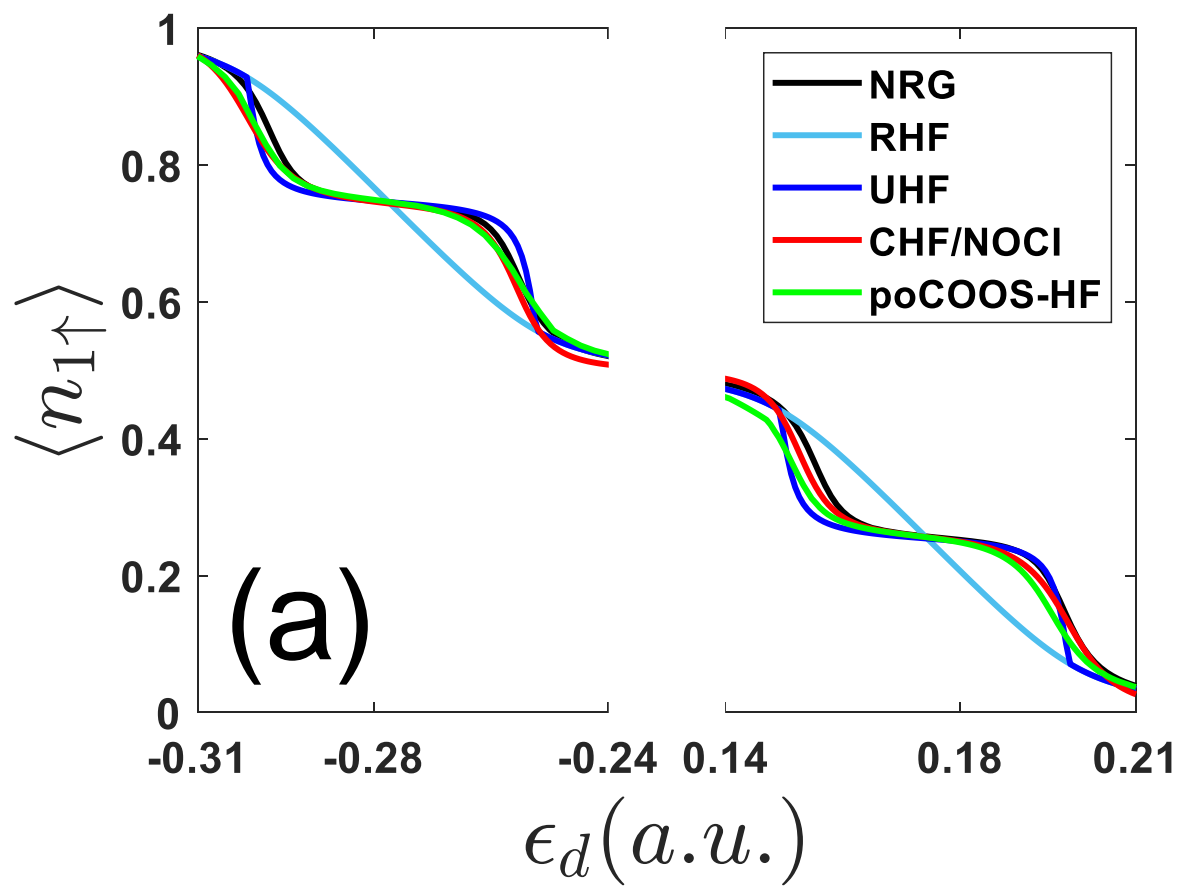
impurity site 1. We set the two impurity energies equal to each other, i.e. $\epsilon_d \equiv \epsilon_{d_1} = \epsilon_{d_2}$. This onsite energy ϵ_d (which is varied along the x -axis) can be considered a charge transfer coordinate. Each plot is separated into two ϵ_d regimes, where the total number of electrons on the impurities range from 4 electrons to 2 electrons and 2 electrons to 0 electron, respectively; note that $\langle n_{tot} \rangle = 4 \langle n_{1\uparrow} \rangle$ for this restricted system. In the following context, these two regimes will be represented as $4 \geq \langle n_{tot} \rangle \geq 2$ and $2 \geq \langle n_{tot} \rangle \geq 0$. The black line is the exact Numerical Renormalization Group (NRG) results for benchmark. The light blue line is restricted Hartree-Fock (RHF). The dark blue line is the unrestricted Hartree-Fock (UHF) result. The red line is constrained Hartree-Fock with non-orthogonal configuration interaction (CHF/NOCI). And lastly, the green line is the partially optimized closed-or-open shell Hartree-Fock (poCOOS-HF) result.

To begin with, consider the performance of the RHF and UHF methods. As one can see in Fig. 1(c), for the strong coupling regime, where static correlation is minimal, RHF itself is already a reasonable approximation to the ground state. However, for the weak or intermediate metal-molecule coupling regime, RHF becomes qualitatively incorrect when static correlation begins to dominate. At this point, UHF does agree pretty well with NRG – but with two obvious disadvantages. First, there is a large discontinuity in the UHF results at the Coulson-Fischer point (see Figs. 1(a,b)). Second, there is spin-contamination problem (which will be discussed in detail in Sec. IVA).

Next, we turn to the CHF/NOCI method. As is well known, one of the disadvantages of CHF(or CDFT) is that the method can fail to describe strongly coupled molecule-metal systems where the subsystem being constrained (in this paper, the two impurity sites) and the unconstrained subsystem (in this paper, the bath) are difficult to distinguish. Thus, the most important test of such a system for CHF/CI will be the strong hybridization case. As can be seen in Fig. 1, while CHF/NOCI (the red line) matches up with NRG pretty well in the weak coupling ($U = 10\Gamma$) and intermediate coupling ($U = 5\Gamma$) regime, the method fails in the strong coupling ($U = \Gamma$) regime.

Lastly, let us address the green curve in Fig. 1, representing the partially optimized closed-or-open shell Hartree Fock (poCOOS-HF) results. As can be seen in Fig. 1, poCOOS-HF results match with NRG results fairly well in the three different coupling regimes. As one would hope, in the weak and intermediate coupling regimes, poCOOS-HF behaves like UHF but with no spin-contamination; whereas in strong coupling regime, poCOOS-HF follows the (smooth) RHF solution. As a side note, we mention that, in Fig. 1(c), where the coupling is so strong that RHF and UHF can be considered close to the exact solution, most of the small offset between the RHF/UHF/ poCOOS-HF results and the NRG results can be attributed to the small systematic error of the NRG method (related to the choice of chain length, logarithmic discretization parameter, temperature parameter and energy truncation²³). (For instance, the NRG approach will not be exactly on top of the RHF line even for $\Gamma = 0$, where RHF is truly exact.) These results are encouraging for future dynamics simulations.

Next, we consider energies. Fig. 2 plots the ground state energy (relative to RHF) as calculated by UHF, CHF/NOCI and poCOOS-HF in three different coupling regimes: (a) $U = 10\Gamma$, (b) $U = 5\Gamma$ and (c) $U = \Gamma$. The x axis is the same as in Fig. 1. One can see from Fig. 2 that the poCOOS-HF energy is very close to UHF and even lower than UHF when $U = 5\Gamma$. Both UHF and poCOOS-HF give a maximum energy correction when $\langle n_{tot} \rangle = 3$ and $\langle n_{tot} \rangle = 1$, in which case the impurity has open-shell singlet character. Interestingly, in Fig. 2(a), even though the CHF/NOCI energy is about $1e-3$ higher than UHF or poCOOS-HF, the CHF/NOCI electron population (in Fig. 1(a)) is still pretty close to the UHF or poCOOS-HF results.



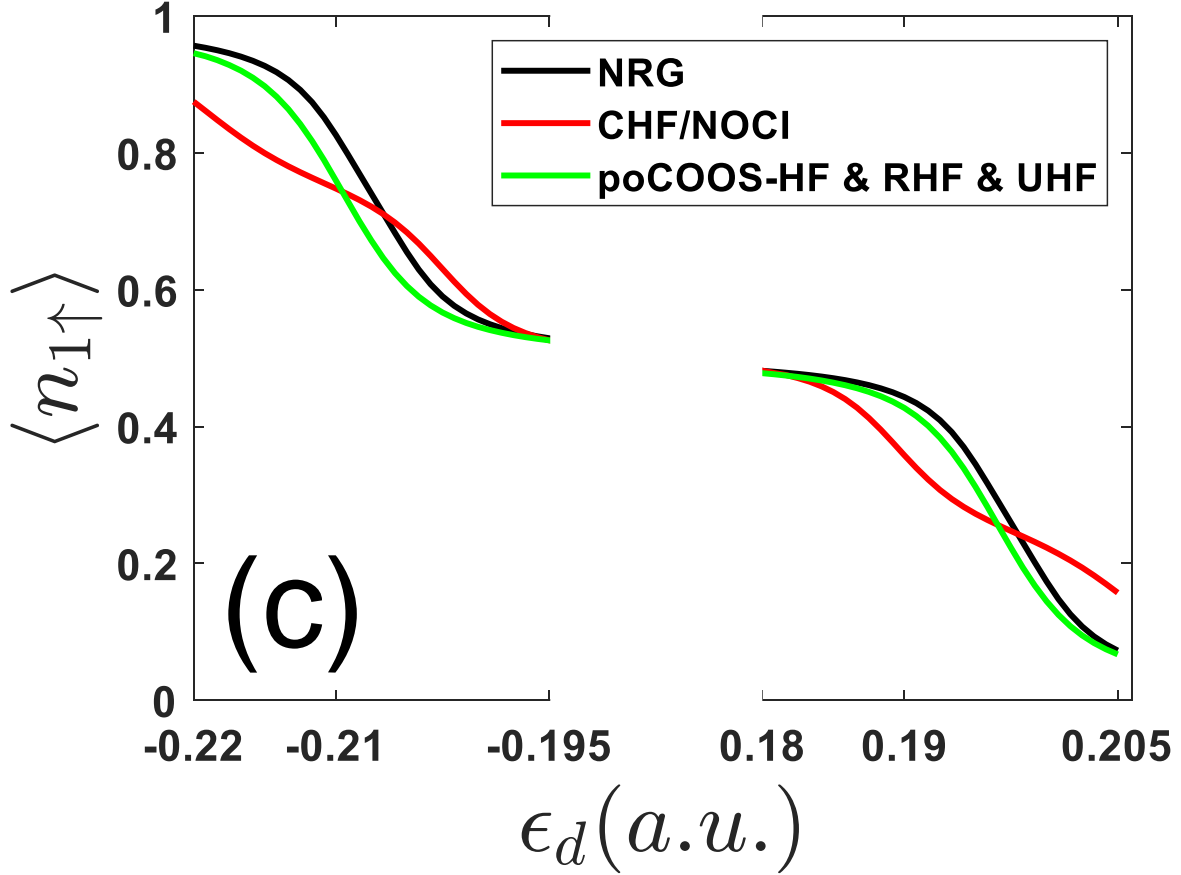
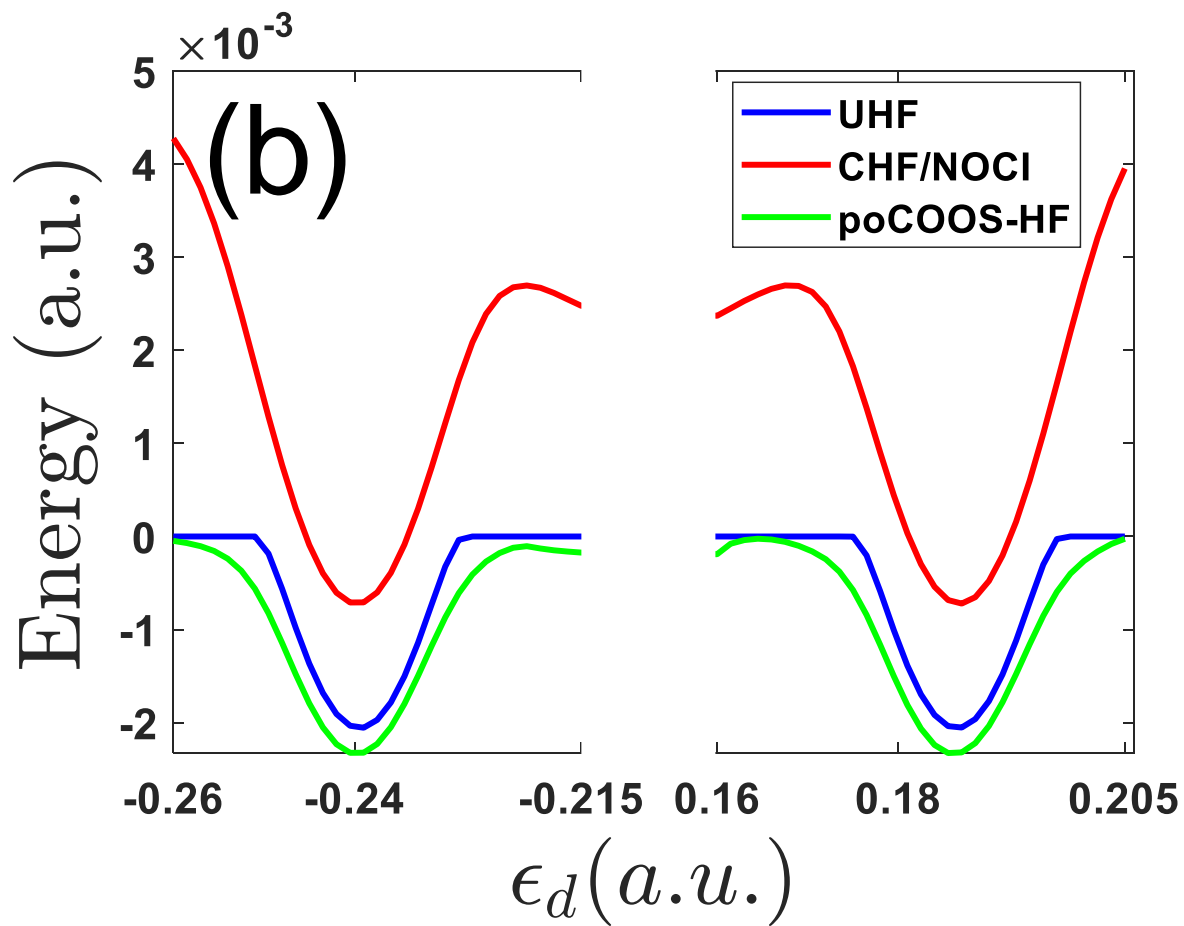
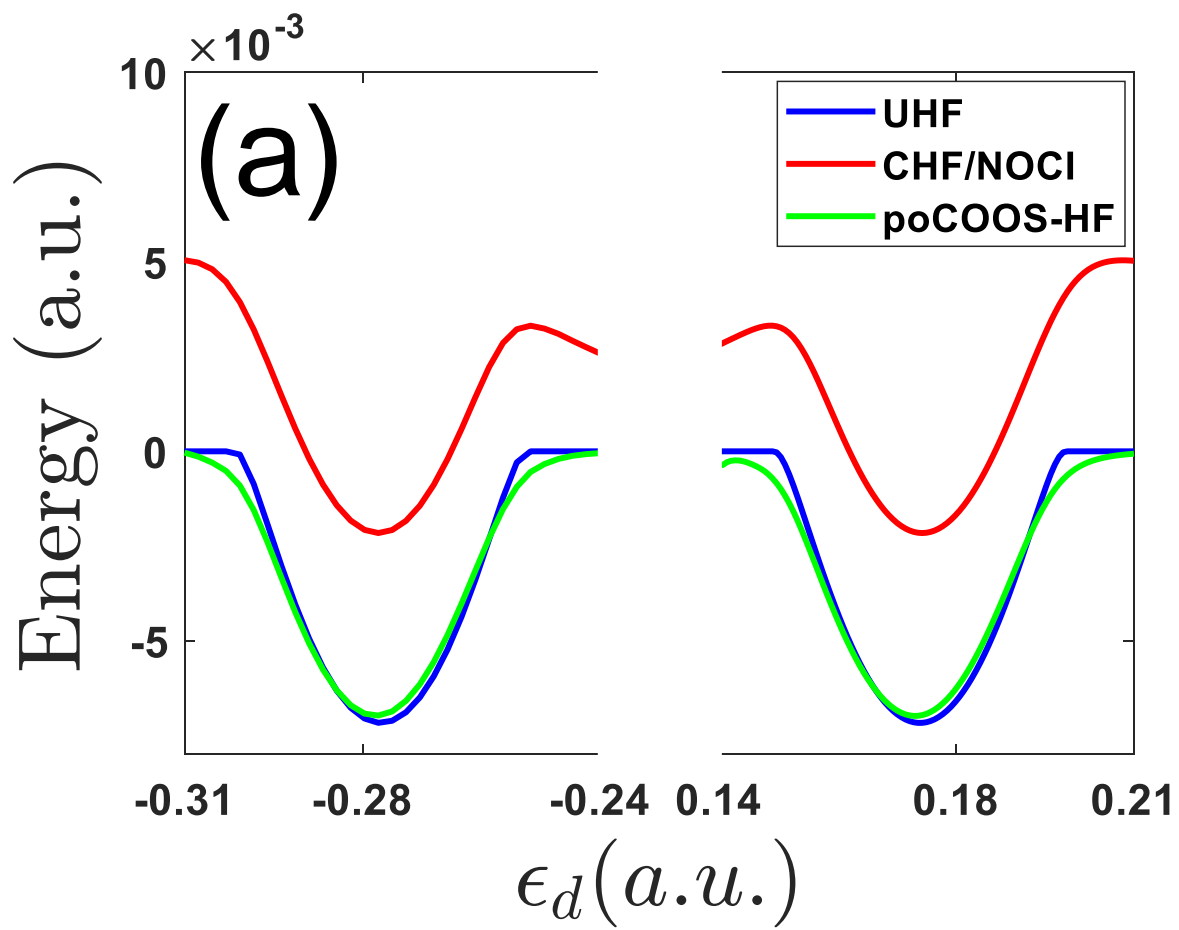


Figure 1: The ground state spin-up electron population on impurity site 1 as a function of the onsite energy $\epsilon_d = \epsilon_{d_1} = \epsilon_{d_2}$, with different onsite repulsion energies. (a) $U = 10\Gamma$; (b) $U = 5\Gamma$; (c) $U = \Gamma$. Note that poCOOS-HF results match NRG results well for all three different onsite repulsion U regimes. Here, the parameters are: $t_d = 0.2$, 803 number of states (801 bath states plus 2 impurities) with band width 0.8 and $\Gamma = 0.01$.



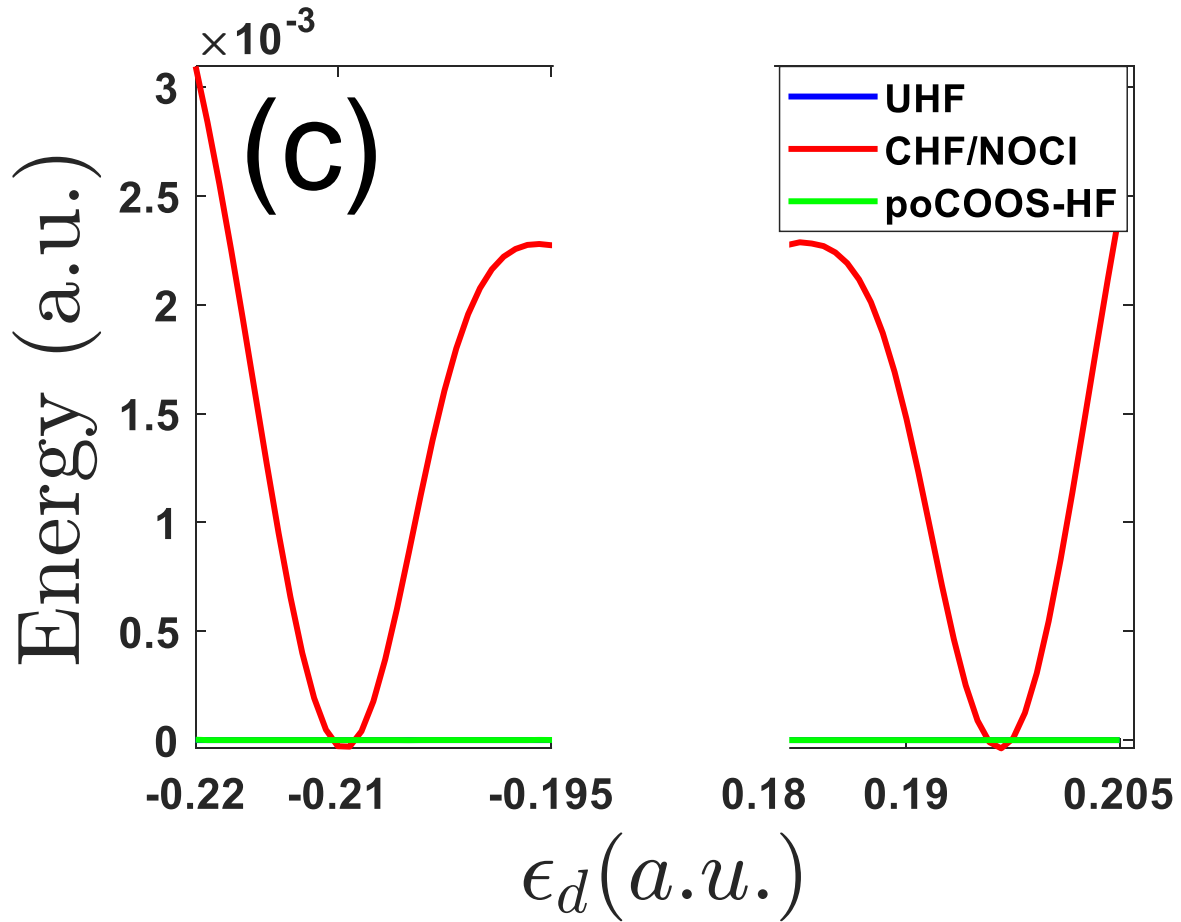


Figure 2: The ground state energy (relative to RHF energy) as a function of the onsite energy ϵ_d , with different onsite repulsion energies. (a) $U = 10\Gamma$; (b) $U = 5\Gamma$; (c) $U = \Gamma$. Note that the poCOOS-HF energy is comparable to the UHF energy for all three different onsite repulsion U regimes. All parameters are the same as in Fig. 1.

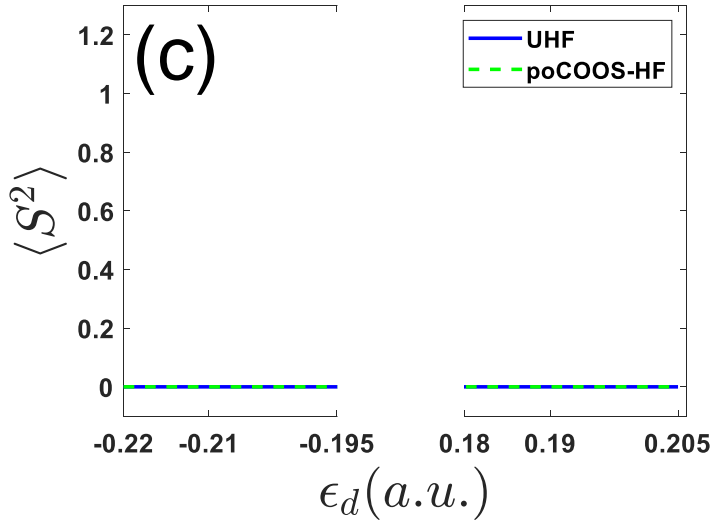
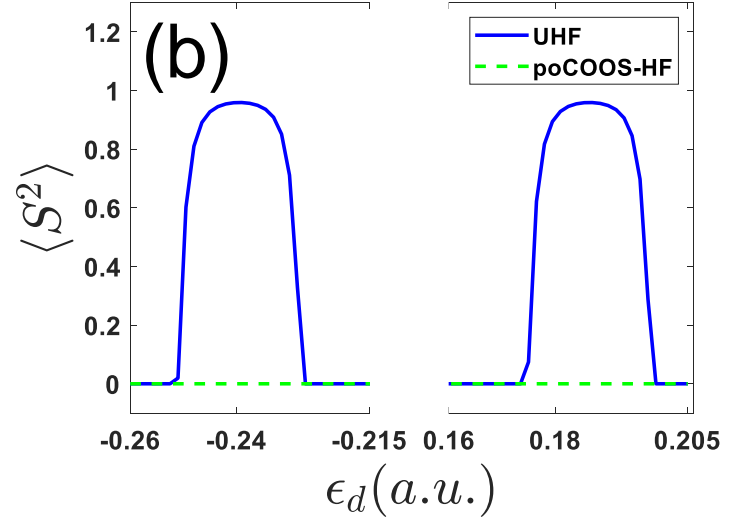
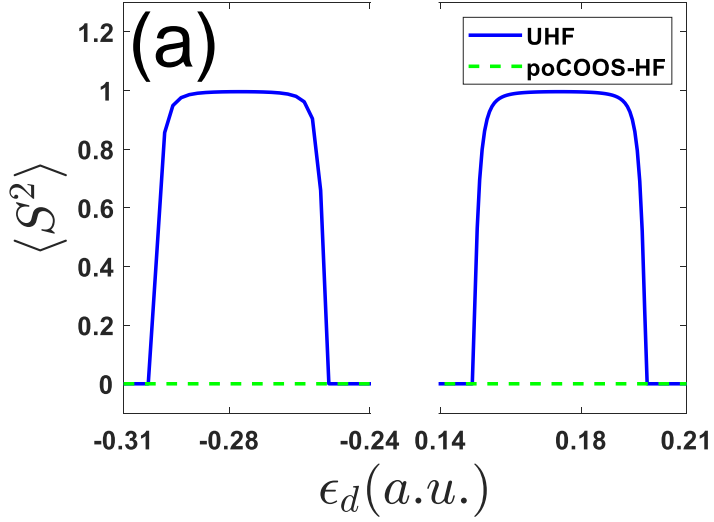


Figure 3: Spin contamination ($\langle S^2 \rangle$) as a function of the onsite energy ϵ_d , with different onsite repulsion energies. (a) $U = 10\Gamma$; (b) $U = 5\Gamma$; (c) $U = \Gamma$. Note that UHF has substantial spin-contamination for $U = 5\Gamma$ and $U = 10\Gamma$. Also note that poCOOS-HF has no spin-contamination because the algorithm works with a pure singlet wavefunction, see Eq. 22. All parameters are the same as in Fig. 1

IV Discussion

A Spin-Contamination

One of the strengths of the poCOOS-HF method is that the method works with a singlet wavefunction, and therefore the method does not have any spin-contamination. By contrast, as is well known, UHF does suffer from substantial spin contamination. In Fig. 3, we report spin-contamination ($\langle S^2 \rangle$) for the three different onsite repulsions U . One can see that for $U = 5\Gamma$ and $U = 10\Gamma$, $\langle S^2 \rangle$ for UHF can be as large as one; large changes in spin contamination arise near the UHF Coulson-Fisher points.

As a practical matter, the poCOOS-HF ansatz was designed to avoid the two problems just listed. Our goal was to seek the simplest spin-pure wavefunction method that could break symmetry (and introduce multi-reference character) in the weak and intermediate coupling, but at the same time recover symmetry in strong coupling limit, all the while being as smooth as possible. For that goal, the two standard candidates in the literature would be: broken symmetry UHF (BS-UHF) and spin-flip (SF) methods. It will be interesting to benchmark the results here versus those approaches in the future. However, already we know that the BS-UHF method is not free of spin contamination. As for spin-flip methods, often one must include more configurations than a standard SF-CIS calculation³⁸⁻⁴⁰ if one wishes to recover a solution free of spin-contamination, e.g. one must implement the SA-SF-CIS method of Zhang and Herbert⁴¹ or the SF-XCIS method of Casanova and Head-Gordon.⁴² Another interesting option to explore in the future would be Holomorphic Hartree-Fock^{43,44} theory where smooth energy curves can be obtained, at least for systems not too large.

B poCOOS vs foCOOS vs CASSCF(2,2)

At this point, we have seen the poCOOS approach can perform fairly well for the Anderson embedding problem. That being said, one can argue that poCOOS-HF is only a partially optimized theory. After all, the algorithm optimizes only 3-orbitals ($\mathbf{o}, \mathbf{p}, \mathbf{q}$ in 23) while the

remaining orbitals are kept in the RHF reference state. In particular, poCOOS-HF optimizes the orbital \mathbf{o} within the RHF occupied space, and the remaining core orbitals are not fully optimized in terms of energy as a function orbital rotation parameters (i.e. κ_{it} and κ_{ia} , where i indexes core orbitals, t indexes active orbitals and a indexes virtual orbitals).

In the future, one can imagine fully optimizing all of the orbitals in the wavefunction of Eq. 18, what we might call a fully optimized foCOOS-HF (see Eq. 18, which optimizes a set of orthogonal orbitals (parametrized by κ_{rs} , where r, s index any orbitals) and CI coefficients (parametrized by α, β, γ in Eq. 31). In this spirit, one can clearly ascertain that the foCOOS ansatz would generate many (but not all) configurations suggested by a CASSCF(2,2) wavefunction. Note that this equivalence is not exact because the parameter space for CASSCF(2,2) CI coefficients is a complete ellipsoid while the parameter space for foCOOS-HF is only a subset of such a CASSCF(2,2) space. To see this constraint clearly, consider Eq. 31, where the normalization constraint can be written as:

$$\alpha^2 + \beta^2 + 2\gamma^2 = 1 \quad (42)$$

This equation can be recast as:

$$(\alpha + \beta)^2 + 2\gamma^2 - 2\alpha\beta = 1 \quad (43)$$

Note that:

$$2\gamma^2 - 2\alpha\beta = 2 \frac{\cos^2 \theta \sin^2 \eta + \sin^2 \theta \cos^2 \eta}{N} \geq 0, \quad (44)$$

so that our COOS-HF ansatz must satisfy:

$$(\alpha + \beta)^2 \leq 1 \quad (45)$$

See Fig. 4. Thus, one can consider the parameter space for foCOOS as a ellipsoid cut by two planes, $\alpha + \beta = -1$ and $\alpha + \beta = 1$, that is clearly only a subset of the CAS space. For

instance, if one considers the CAS parameter set $\{\alpha = \beta = \frac{1}{\sqrt{2}}, \gamma = 0\}$, clearly there is no corresponding $\{\theta, \eta\}$ COOS-HF parameter set.

While one might argue that this limitation represents a failure of the COOS-HF wavefunction (because a bigger variational space is always better), we are hopeful that this will not be the case. First, because we have fewer degrees of freedom, we are hopeful that a foCOOS-HF wavefunction (as constructed exclusively from a set of meaningful orbitals), we will be able to build a balanced reference for ground and excited state calculations *without state averaging*. Second, we are also hopeful that using our choice of frontier orbitals, future work with non-orthogonal configuration interaction Hamiltonians (for excited states) will require smaller diagonalizations and few multireference problems. Third, we are also hopeful that with fewer degrees of freedom, there will be fewer discontinuities to deal with dynamically (and in particular, the code can be run without manually choosing an active space).

As an example of a situation we might expect to encounter, consider the case where we expect the wavefunction to have half occupation for highest occupied molecular orbital (HOMO) and a half occupation for the lowest unoccupied molecular orbital (LUMO), in other words a one-electron density matrix D of the form:

$$D = \sum_{i \in \text{core}} |i\rangle \langle i| + \frac{1}{2} |h\rangle \langle h| + \frac{1}{2} |l\rangle \langle l| \quad (46)$$

In order to represent such a density matrix within a CAS parameter space, there are two possible wavefunctions: $\{\alpha = \beta = 0, \gamma = \frac{1}{\sqrt{2}}\}$ ($\frac{1}{\sqrt{2}}(|h\bar{l}\rangle + |l\bar{h}\rangle)$) and $\{\alpha = \beta = \frac{1}{\sqrt{2}}, \gamma = 0\}$ ($\frac{1}{\sqrt{2}}(|h\bar{h}\rangle + |l\bar{l}\rangle)$). In the future, it will be interesting to check if CAS calculations converge to the same minimum starting from these two different starting guesses. That being said, since the parameter set $\{\alpha = \beta = \frac{1}{\sqrt{2}}, \gamma = 0\}$ is out of the COOS-HF parameter space, foCOOS will only have one unique guess wavefunction, i.e. $\frac{1}{\sqrt{2}}(|h\bar{l}\rangle + |l\bar{h}\rangle)$, and so is less likely to suffer multiple solutions. In short, the essence of the present approach is that we are willing

to deal with less accuracy (i.e. not including a full CAS space) if our goal is really to run nonadiabatic dynamics over a smooth and qualitatively correct surface. This same reasoning explains why many dynamicists over prefer CASCI to CASSCF for many applications.⁴⁵

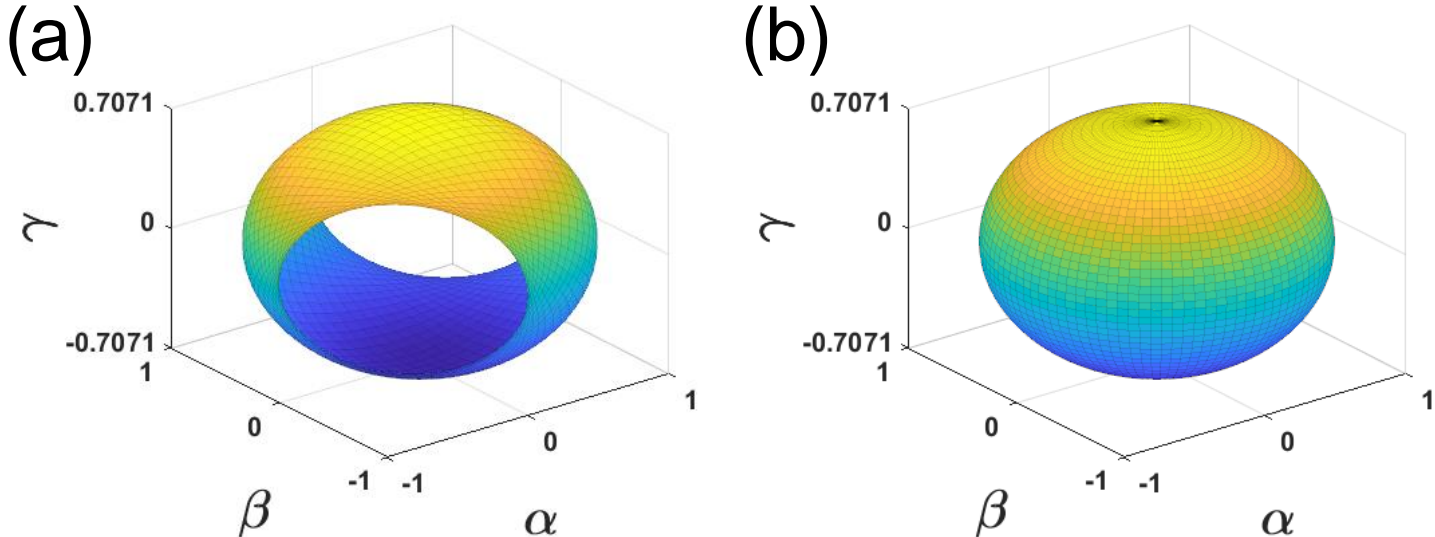


Figure 4: CI coefficients parameter space for (a) COOS-HF; (b) CASSCF(2,2). Note that the CASSCF(2,2) parameter space forms a complete ellipsoid ($\alpha^2 + \beta^2 + 2\gamma^2 = 1$) with semi-axes of $(1, 1, \frac{1}{\sqrt{2}})$ while COOS-HF covers just a part of this ellipsoid. The forbidden part of the COOS-HF parameter space corresponds to the areas $\{\alpha > 0, \beta > 0\}$ and $\{\alpha < 0, \beta < 0\}$.

V Discussion and Conclusion

In summary, we have presented a straightforward closed or open shell HF approach for electronic structure theory and we have compared such an approach against a CHF/NOCI ansatz for the two-site Anderson model of a molecule sitting on a metal surface. We have tested the algorithms in the weak ($U = 10\Gamma$), intermediate ($U = 5\Gamma$) and strong ($U = \Gamma$) coupling regimes and we have found that poCOOS-HF can obtain accurate results as compared with exact numerical renormalization group (NRG) theory, recovering charge transfer states where appropriate; in particular, in the weak and intermediate coupling regimes, poCOOS-HF can recover the strong open-shell singlet character (when $\langle n_{tot} \rangle = 3$ and $\langle n_{tot} \rangle = 1$) exhibited by the impurity.

Looking forward, the COOS-HF approach has the attractive feature that the algorithm can be completely characterized by a set of orbitals, i.e. one does not need to list any CI coefficients. As such, the ansatz may prove amenable to a merger with DFT. Moreover, in the future, one would like to run molecule non-adiabatic dynamics on metal surfaces through the current framework. Progress on this front will depend on two important future developments. First, if one looks very carefully at Fig. 1(a), in the strong U regime, poCOOS-HF would appear to have four small discontinuities around $\epsilon = -0.30, -0.25, 0.15, 0.20$, attributable to a Coulson-Fischer point (similar to UHF). The changes in slope are clearly far smaller for poCOOS-HF than for UHF, but they may be unavoidable. One would hope that, if one implements the fo-COOS-HF approach, such a discontinuity will be removed entirely. Second, in the future, it will be essential to generate excited states on top of a COOS-HF reference. Again, it will be essential to generate smooth surfaces as much as possible. Despite these concerns, all indications are that the present approach has the potential to be applied to reasonably sized electronic subsystems interacting with large electronic baths for use in future dynamical approaches.

Acknowledgement

This work was supported by the U.S. Air Force Office of Scientific Research (USAFOSR) under Grant Nos. FA9550-18-1-0497 and FA9550-18-1-0420. We thank the DoD High Performance Computing Modernization Program for computer time. And we also thank the Texas Advanced Computing Center (TACC) at The University of Texas at Austin for providing HPC resources that have contributed to the research results reported in this paper. URL: <http://www.tacc.utexas.edu>

VI Appendix

A Non-Orthogonal Configuration Matrix Element

Under the framework of constrained Hartree-Fock, suppose we find two ground states with the total number of electrons on the impurities equal to 0 and 1, denoted as $\langle \Phi_g | \sum_{\sigma} d_{1\sigma}^{\dagger} d_{1\sigma} + d_{2\sigma}^{\dagger} d_{2\sigma} | \Phi_g \rangle = 1$ and $\langle \Phi'_g | \sum_{\sigma} d_{1\sigma}^{\dagger} d_{1\sigma} + d_{2\sigma}^{\dagger} d_{2\sigma} | \Phi'_g \rangle = 0$. The quantity that we want to calculate is the matrix element: $\langle \Phi_g | H | \Phi'_g \rangle$. In the following paragraph, the one electron operator $d^{\dagger} b$ will be used to derive such non-orthogonal matrix elements; here, d^{\dagger} represents the impurity atomic orbital and b^{\dagger} represents the bath atomic orbital.

The matrix element we wish to calculate can be explicitly written as: $\langle \Phi_g | \sum_b \sum_{\sigma} d_{1\sigma}^{\dagger} b_{\sigma} + c.c. | \Phi'_g \rangle$. For restricted orbitals, we can ignore the summation over spin σ and focus on $\langle \Phi_g | 2 \sum_b d_1^{\dagger} b + c.c. | \Phi'_g \rangle$:

$$\langle \Phi_g | \sum_b d_1^{\dagger} b | \Phi'_g \rangle = \langle \Phi_g | \sum_b d_1^{\dagger} b | \Phi_g \rangle \langle \Phi_g | \Phi'_g \rangle + \sum_{ia} \langle \Phi_g | \sum_b d_1^{\dagger} b | \Phi_i^a \rangle \langle \Phi_i^a | \Phi'_g \rangle \quad (47)$$

First of all, using second quantization, it is clear that:

$$\langle \Phi_g | \sum_b d_1^{\dagger} b | \Phi_g \rangle = \sum_b \sum_i^{occ} \langle d_1 | i \rangle \langle i | b \rangle \quad (48)$$

$$\langle \Phi_g | \sum_b d_1^{\dagger} b | \Phi_i^a \rangle = \sum_b \langle d_1 | i \rangle \langle a | b \rangle \quad (49)$$

Secondly, let us calculate the overlap:

$$\langle \Phi_g | \Phi'_g \rangle = \det(S^o) \quad (50)$$

Here, S^o is the N_o by N_o occupied orbital overlap matrix (where N_o is the number of occupied orbitals). To calculate the overlap $\langle \Phi_i^a | \Phi'_g \rangle$, we need to introduce a biorthogonal basis set. If we perform a singular value decomposition on the (occupied-occupied) S^o and (virtual-virtual) S^v overlap matrices,

$$S^o = U^o \Lambda^o V^{o\dagger} \quad (51)$$

$$S^v = U^v \Lambda^v V^{v\dagger}, \quad (52)$$

then the molecular orbitals can be expressed in this biorthogonal basis set:

$$|i\rangle = \sum_k^{occ} |\tilde{k}\rangle U_{ik}^{o*} \quad (53)$$

$$|a\rangle = \sum_c^{vir} |\tilde{c}\rangle U_{ac}^{v*} \quad (54)$$

$$|i'\rangle = \sum_k^{occ} |\tilde{k}'\rangle V_{ik}^{o*} \quad (55)$$

$$|a'\rangle = \sum_c^{vir} |\tilde{c}'\rangle V_{ac}^{v*} \quad (56)$$

We can then express the overlap in this basis of biorthogonal orbitals:

$$\langle \Phi_i^a | \Phi_g' \rangle = \sum_k^{occ} \sum_c^{vir} U_{ac}^v U_{ik}^{o*} \langle \Phi_{\tilde{k}}^{\tilde{c}} | \Phi_{\tilde{g}}' \rangle = \sum_k^{occ} \sum_c^{vir} U_{ac}^v U_{ik}^{o*} \frac{\det(S^o) \langle \tilde{c} | \tilde{k}' \rangle}{\lambda_k} = \sum_k^{occ} U_{ik}^{o*} \frac{\det(S^o) \langle a | \tilde{k}' \rangle}{\lambda_k} \quad (57)$$

The second equality uses the fact that $\det(S^o) = \langle \Phi_g | \Phi_g' \rangle = \langle \Phi_{\tilde{g}} | \Phi_{\tilde{g}}' \rangle = \prod_k^{occ} \lambda_k$ with λ_k being the diagonal element of Λ^o .

Next, the expression above can be simplified again using the identity:

$$\begin{aligned} \sum_k^{occ} U_{ik}^{o*} \frac{1}{\lambda_k} |\tilde{k}'\rangle &= \sum_{kl}^{occ} U_{ik}^{o*} \frac{\delta_{kl}}{\lambda_k} |\tilde{l}'\rangle = \sum_{klm}^{occ} U_{ik}^{o*} \frac{1}{\lambda_k} (V^{o*\dagger})_{km} V_{ml}^{o*} |\tilde{l}'\rangle = \sum_{km}^{occ} U_{ik}^{o*} \frac{1}{\lambda_k} (V^{o*\dagger})_{km} |m'\rangle \\ &= \sum_m^{occ} (V^o \frac{1}{\Lambda^o} U^{o\dagger})_{mi} |m'\rangle = \sum_m^{occ} (S^o)^{-1}_{mi} |m'\rangle \end{aligned} \quad (58)$$

If we substitute Eq.58 into Eq.57, we find:

$$\langle \Phi_i^a | \Phi'_g \rangle = \det(S^o) \sum_m^{occ} (S^o)_{mi}^{-1} \langle a | m' \rangle \quad (59)$$

Finally, by combining Eq.50 and Eq.48, we evaluate the first term of Eq.47.

$$\langle \Phi_g | \sum_b d_1^\dagger b | \Phi_g \rangle \langle \Phi_g | \Phi'_g \rangle = \det(S^o) \sum_{b \in bath} \sum_i^{occ} \langle d_1 | i \rangle \langle i | b \rangle \quad (60)$$

And by combining Eq.59 and Eq.49, we can also evaluate the second term of Eq.47.

$$\begin{aligned} \sum_{ia} \langle \Phi_g | \sum_b d_1^\dagger b | \Phi_i^a \rangle \langle \Phi_i^a | \Phi'_g \rangle &= \det(S^o) \sum_{ia} \sum_b \langle d_1 | i \rangle \langle a | b \rangle \sum_m^{occ} (S^o)_{mi}^{-1} \langle a | m' \rangle \\ &= \det(S^o) \sum_b \sum_{ia} \sum_m^{occ} \langle b | a \rangle \langle a | m' \rangle (S^o)_{mi}^{-1} \langle i | d_1 \rangle \\ &= \det(S^o) \sum_b \sum_i \sum_m^{occ} \langle b | m' \rangle (S^o)_{mi}^{-1} \langle i | d_1 \rangle \\ &\quad - \det(S^o) \sum_b \sum_i^{occ} \langle b | i \rangle \langle i | d_1 \rangle \end{aligned} \quad (61)$$

The third equality uses the property that

$$\sum_a^{vir} |a\rangle\langle a| = I - \sum_j^{occ} |j\rangle\langle j| \quad (62)$$

$$\sum_m^{occ} \langle j | m' \rangle (S^o)_{mi}^{-1} = \sum_m^{occ} (S^o)_{jm} (S^o)_{mi}^{-1} = \delta_{ji} \quad (63)$$

Altogether, by substituting Eq.60 and Eq.61 into Eq.47, we recover

$$\langle \Phi_g | \sum_b d_1^\dagger b | \Phi'_g \rangle = \det(S^o) \sum_{b \in bath} \sum_{im}^{occ} \langle b | m' \rangle (S^o)_{mi}^{-1} \langle i | d_1 \rangle \quad (64)$$

Now we turn to the two-electron operator contribution:

$$\begin{aligned}
\langle \Phi_g | d^\dagger d \bar{d}^\dagger \bar{d} | \Phi'_g \rangle &= \langle \Phi_g | d^\dagger d (|\Phi_g\rangle \langle \Phi_g| + |\Phi_i^a\rangle \langle \Phi_i^a|) \left(|\Phi'_g\rangle \langle \Phi'_g| + |\Phi_{j'}^{b'}\rangle \langle \Phi_{j'}^{b'}| \right) \bar{d}^\dagger \bar{d} | \Phi'_g \rangle \\
&= \langle \Phi_g | d^\dagger d | \Phi_g \rangle \langle \Phi_g | \Phi'_g \rangle \langle \Phi'_g | \bar{d}^\dagger \bar{d} | \Phi'_g \rangle \\
&+ \langle \Phi_g | d^\dagger d | \Phi_g \rangle \langle \Phi_g | \Phi_{j'}^{b'} \rangle \langle \Phi_{j'}^{b'} | \bar{d}^\dagger \bar{d} | \Phi'_g \rangle \\
&+ \langle \Phi_g | d^\dagger d | \Phi_i^a \rangle \langle \Phi_i^a | \Phi'_g \rangle \langle \Phi'_g | \bar{d}^\dagger \bar{d} | \Phi'_g \rangle \\
&+ \langle \Phi_g | d^\dagger d | \Phi_i^a \rangle \langle \Phi_i^a | \Phi_{j'}^{b'} \rangle \langle \Phi_{j'}^{b'} | \bar{d}^\dagger \bar{d} | \Phi'_g \rangle
\end{aligned} \tag{65}$$

where i, j, a, b are dummy summation indices. Then, we define:

$$\begin{aligned}
n_g &= \langle \Phi_g | d^\dagger d | \Phi_g \rangle \\
n_{g'} &= \langle \Phi_{g'} | d^\dagger d | \Phi_{g'} \rangle
\end{aligned} \tag{66}$$

Then, it follows that:

$$\begin{aligned}
&\langle \Phi_g | d^\dagger d | \Phi_g \rangle \langle \Phi_g | \Phi'_g \rangle \langle \Phi'_g | \bar{d}^\dagger \bar{d} | \Phi'_g \rangle = \det(S^o) n_g n_{g'} \\
&\sum_{j'}^{occ} \sum_{b'}^{vir} \langle \Phi_g | d^\dagger d | \Phi_g \rangle \langle \Phi_g | \Phi_{j'}^{b'} \rangle \langle \Phi_{j'}^{b'} | \bar{d}^\dagger \bar{d} | \Phi'_g \rangle = \det(S^o) n_g \sum_{ij'}^{occ} \langle d | j' \rangle (S^o)_{ji}^{-1} \langle i | d \rangle - \det(S^o) n_g n_{g'} \\
&\sum_i^{occ} \sum_a^{vir} \langle \Phi_g | d^\dagger d | \Phi_i^a \rangle \langle \Phi_i^a | \Phi'_g \rangle \langle \Phi'_g | \bar{d}^\dagger \bar{d} | \Phi'_g \rangle = \det(S^o) n_{g'} \sum_{ij'}^{occ} \langle d | j' \rangle (S^o)_{ji}^{-1} \langle i | d \rangle - \det(S^o) n_g n_{g'} \\
&\sum_{ij'}^{occ} \sum_{ab'}^{vir} \langle \Phi_g | d^\dagger d | \Phi_i^a \rangle \langle \Phi_i^a | \Phi_{j'}^{b'} \rangle \langle \Phi_{j'}^{b'} | \bar{d}^\dagger \bar{d} | \Phi'_g \rangle = \det(S^o) \sum_{im'}^{occ} \langle d | m' \rangle (S^o)_{mi}^{-1} \langle i | d \rangle \sum_{kj'}^{occ} \langle d | j' \rangle (S^o)_{jk}^{-1} \langle k | d \rangle \\
&\quad - \det(S^o) n_g \sum_{kj'}^{occ} \langle d | j' \rangle (S^o)_{jk}^{-1} \langle k | d \rangle \\
&\quad - \det(S^o) n_{g'} \sum_{im'}^{occ} \langle d | m' \rangle (S^o)_{mi}^{-1} \langle i | d \rangle \\
&\quad + \det(S^o) n_g n_{g'}
\end{aligned} \tag{67}$$

Altogether, there is a lot of cancellation, and the two-electron operator contribution is:

$$\langle \Phi_g | d^\dagger d \bar{d}^\dagger \bar{d} | \Phi'_g \rangle = \det(S^o) \sum_{im'}^{occ} \langle d|m' \rangle (S^o)_{m'i}^{-1} \langle i|d \rangle \sum_{kj'}^{occ} \langle d|j' \rangle (S^o)_{j'k}^{-1} \langle k|d \rangle \quad (68)$$

B Analytical Energy Gradient for poCOOS-HF

Lastly, for the sake of completeness, here we list all of the electronic derivatives (with respect to orbital variations) of the relevant fock operators, overlap matrix elements, and two electron matrix elements as present in Eq. 37.

B.1 Derivatives of Fock Operators

$$\frac{\partial f_{oo}}{\partial c_i} = 2 \sum_j c_j f_{ij} \quad (69)$$

$$\begin{aligned} \frac{\partial f_{pp}}{\partial c_i} &= d_o^2 \cdot 2 \sum_j c_j f_{ij} + 2 \sum_a d_o d_a f_{ia} \\ \frac{\partial f_{pp}}{\partial d_o} &= 2 d_o \sum_{ij} c_i c_j f_{ij} + 2 \sum_a d_a \sum_i c_i f_{ia} \\ \frac{\partial f_{pp}}{\partial d_a} &= 2 d_o \sum_i c_i f_{ia} + 2 \sum_b d_b f_{ab} \end{aligned} \quad (70)$$

$$\begin{aligned} \frac{\partial f_{qq}}{\partial c_i} &= \tilde{d}_o^2 \cdot 2 \sum_j c_j f_{ij} + 2 \sum_a \tilde{d}_o \tilde{d}_a f_{ia} \\ \frac{\partial f_{qq}}{\partial \tilde{d}_o} &= 2 \tilde{d}_o \sum_{ij} c_i c_j f_{ij} + 2 \sum_a \tilde{d}_a \sum_i c_i f_{ia} \\ \frac{\partial f_{qq}}{\partial \tilde{d}_a} &= 2 \tilde{d}_o \sum_i c_i f_{ia} + 2 \sum_b \tilde{d}_b f_{ab} \end{aligned} \quad (71)$$

$$\begin{aligned}
\frac{\partial f_{pq}}{\partial c_i} &= d_o \tilde{d}_o \cdot 2 \sum_j c_j f_{ij} + \sum_a \tilde{d}_o d_a f_{ia} + \sum_a d_o \tilde{d}_a f_{ia} \\
\frac{\partial f_{pq}}{\partial d_o} &= \tilde{d}_o \sum_{ij} c_i c_j f_{ij} + \sum_a \tilde{d}_a \sum_i c_i f_{ia} \\
\frac{\partial f_{pq}}{\partial \tilde{d}_o} &= d_o \sum_{ij} c_i c_j f_{ij} + \sum_a d_a \sum_i c_i f_{ia} \\
\frac{\partial f_{pq}}{\partial d_a} &= \tilde{d}_o \sum_i c_i f_{ia} + \sum_b \tilde{d}_b f_{ab} \\
\frac{\partial f_{pq}}{\partial \tilde{d}_a} &= d_o \sum_i c_i f_{ia} + \sum_b d_b f_{ab}
\end{aligned} \tag{72}$$

B.2 Derivatives of Overlap Matrices

$$\begin{aligned}
\frac{\partial \langle p|q \rangle}{\partial c_i} &= d_o \tilde{d}_o \cdot 2c_i + \sum_a d_o \tilde{d}_a \langle i|a \rangle + \sum_a \tilde{d}_o d_a \langle i|a \rangle \\
\frac{\partial \langle p|q \rangle}{\partial d_o} &= \tilde{d}_o \sum_i c_i^2 + \sum_{ai} \tilde{d}_a c_i \langle i|a \rangle \\
\frac{\partial \langle p|q \rangle}{\partial \tilde{d}_o} &= d_o \sum_i c_i^2 + \sum_{ai} d_a c_i \langle i|a \rangle \\
\frac{\partial \langle p|q \rangle}{\partial d_a} &= \sum_b \tilde{d}_b \langle a|b \rangle + \sum_i \tilde{d}_o c_i \langle i|a \rangle \\
\frac{\partial \langle p|q \rangle}{\partial \tilde{d}_a} &= \sum_b d_b \langle b|a \rangle + \sum_i d_o c_i \langle i|a \rangle
\end{aligned} \tag{73}$$

B.3 Derivatives of Two Electron Integrals

$$\frac{\partial(o o|o o)}{\partial c_i} = 4 \sum_{jkl} c_j c_k c_l (ij|kl) \tag{74}$$

$$\begin{aligned}
\frac{\partial(pq|qp)}{\partial c_i} &= d_o^2 \tilde{d}_o^2 \sum_{jkl} 4c_j c_k c_l (ij|kl) \\
&+ (d_o^2 \cdot 2 \sum_a \tilde{d}_a \tilde{d}_a + 2 \sum_a d_o d_a \cdot \tilde{d}_o^2) \cdot \sum_{jk} 3c_j c_k (ij|ka) \\
&+ (d_o^2 \cdot \sum_{ab} \tilde{d}_a \tilde{d}_b + 2 \sum_a d_o d_a \cdot 2 \sum_b \tilde{d}_o \tilde{d}_b + \sum_{ab} d_a d_b \cdot \tilde{d}_o^2) \cdot \sum_j 2c_j (ij|ab) \\
&+ (2 \sum_a d_o d_a \cdot \sum_{bc} \tilde{d}_b \tilde{d}_c + \sum_{ab} d_a d_b \cdot 2 \sum_c \tilde{d}_o \tilde{d}_c) \cdot (ia|bc)
\end{aligned} \tag{75}$$

$$\begin{aligned}
\frac{\partial(pq|qp)}{\partial d_o} &= 2d_o \tilde{d}_o^2 \sum_{ijkl} c_i c_j c_k c_l (ij|kl) \\
&+ (2d_o \cdot 2 \sum_a \tilde{d}_o \tilde{d}_a + 2 \sum_a d_a \cdot \tilde{d}_o^2) \cdot \sum_{ijk} c_i c_j c_k (ij|ka) \\
&+ (2d_o \cdot \sum_{ab} \tilde{d}_a \tilde{d}_b + 2 \sum_a d_a \cdot 2 \sum_b \tilde{d}_o \tilde{d}_b) \cdot \sum_{ij} c_i c_j (ij|ab) \\
&+ (2 \sum_a d_a \cdot \sum_{bc} \tilde{d}_b \tilde{d}_c) \cdot \sum_i c_i (ia|bc)
\end{aligned} \tag{76}$$

$$\begin{aligned}
\frac{\partial(pq|qp)}{\partial d_a} &= (2d_o \cdot \tilde{d}_o^2) \cdot \sum_{ijk} c_i c_j c_k (ij|ka) \\
&+ (2d_o \cdot 2 \sum_b \tilde{d}_o \tilde{d}_b + \sum_b 2d_b \cdot \tilde{d}_o^2) \cdot \sum_{ij} c_i c_j (ij|ab) \\
&+ (2d_o \cdot \sum_{bc} \tilde{d}_b \tilde{d}_c + \sum_b 2d_b \cdot 2 \sum_c \tilde{d}_o \tilde{d}_c) \cdot \sum_i c_i (ia|bc) \\
&+ \sum_b 2d_b \cdot \sum_{cd} \tilde{d}_c \tilde{d}_d (ab|cd)
\end{aligned} \tag{77}$$

$$\begin{aligned}
\frac{\partial(pq|qp)}{\partial \tilde{d}_o} &= 2d_o^2 \tilde{d}_o \sum_{ijkl} c_i c_j c_k c_l (ij|kl) \\
&+ (d_o^2 \cdot 2 \sum_a \tilde{d}_a + 2 \sum_a d_o d_a \cdot 2\tilde{d}_o) \cdot \sum_{ijk} c_i c_j c_k (ij|ka) \\
&+ (2 \sum_a d_o d_a \cdot 2 \sum_b \tilde{d}_b + \sum_{ab} d_a d_b \cdot 2\tilde{d}_o) \cdot \sum_{ij} c_i c_j (ij|ab) \\
&+ (\sum_{ab} d_a d_b \cdot 2 \sum_c \tilde{d}_c) \cdot \sum_i c_i (ia|bc)
\end{aligned} \tag{78}$$

$$\begin{aligned}
\frac{\partial(pq|qp)}{\partial \tilde{d}_b} &= (d_o^2 \cdot 2\tilde{d}_o) \cdot \sum_{ijk} c_i c_j c_k (ij|kb) \\
&+ (d_o^2 \cdot \sum_a 2\tilde{d}_a + 2 \sum_a d_o d_a \cdot 2\tilde{d}_o) \cdot \sum_{ij} c_i c_j (ij|ab) \\
&+ (2 \sum_a d_o d_a \cdot \sum_c 2\tilde{d}_c + \sum_{ac} d_a d_c \cdot 2\tilde{d}_o) \cdot \sum_i c_i (ia|cb) \\
&+ \sum_{ac} d_a d_c \cdot \sum_d 2\tilde{d}_d (ac|bd)
\end{aligned} \tag{79}$$

$$\begin{aligned}
\frac{\partial(o_o|pp)}{\partial c_i} &= d_o^2 \cdot \sum_{jkl} 4c_j c_k c_l (ij|kl) + 2 \sum_a d_o d_a \cdot \sum_{jk} 3c_j c_k (ij|ka) + \sum_{ab} d_a d_b \cdot \sum_j 2c_j (ij|ab) \\
\frac{\partial(o_o|pp)}{\partial d_o} &= 2d_o \cdot \sum_{ijkl} c_i c_j c_k c_l (ij|kl) + 2 \sum_a d_a \cdot \sum_{ijk} c_i c_j c_k (ij|ka) \\
\frac{\partial(o_o|pp)}{\partial d_a} &= 2d_o \cdot \sum_{ijk} c_i c_j c_k (ij|ka) + \sum_b 2d_b \cdot \sum_{ij} c_i c_j (ij|ab)
\end{aligned} \tag{80}$$

$$\begin{aligned}
\frac{\partial(o_o|qq)}{\partial c_i} &= \tilde{d}_o^2 \cdot \sum_{jkl} 4c_j c_k c_l (ij|kl) + 2 \sum_a \tilde{d}_o \tilde{d}_a \cdot \sum_{jk} 3c_j c_k (ij|ka) + \sum_{ab} \tilde{d}_a \tilde{d}_b \cdot \sum_j 2c_j (ij|ab) \\
\frac{\partial(o_o|qq)}{\partial \tilde{d}_o} &= 2\tilde{d}_o \cdot \sum_{ijkl} c_i c_j c_k c_l (ij|kl) + 2 \sum_a \tilde{d}_a \cdot \sum_{ijk} c_i c_j c_k (ij|ka) \\
\frac{\partial(o_o|qq)}{\partial \tilde{d}_a} &= 2\tilde{d}_o \cdot \sum_{ijk} c_i c_j c_k (ij|ka) + \sum_b 2\tilde{d}_b \cdot \sum_{ij} c_i c_j (ij|ab)
\end{aligned} \tag{81}$$

$$\begin{aligned}
\frac{\partial(o_o|pq)}{\partial c_i} &= d_o \tilde{d}_o \cdot \sum_{jkl} 4c_i c_j c_k c_l (ij|kl) + \sum_a (d_a \tilde{d}_o + d_o \tilde{d}_a) \cdot \sum_{jk} 3c_i c_j c_k (ij|ka) + \sum_{ab} d_a \tilde{d}_b \cdot \sum_{ij} 2c_j (ij|ab) \\
\frac{\partial(o_o|pq)}{\partial d_o} &= \tilde{d}_o \cdot \sum_{ijkl} c_i c_j c_k c_l (ij|kl) + \sum_a \tilde{d}_a \cdot \sum_{ijk} c_i c_j c_k (ij|ka) \\
\frac{\partial(o_o|pq)}{\partial \tilde{d}_o} &= d_o \cdot \sum_{ijkl} c_i c_j c_k c_l (ij|kl) + \sum_a d_a \cdot \sum_{ijk} c_i c_j c_k (ij|ka) \\
\frac{\partial(o_o|pq)}{\partial d_a} &= \tilde{d}_o \cdot \sum_{ijk} c_i c_j c_k (ij|ka) + \sum_b \tilde{d}_b \cdot \sum_{ij} c_i c_j (ij|ab) \\
\frac{\partial(o_o|pq)}{\partial \tilde{d}_a} &= d_o \cdot \sum_{ijk} c_i c_j c_k (ij|ka) + \sum_b d_b \cdot \sum_{ij} c_i c_j (ij|ab)
\end{aligned} \tag{82}$$

References

- (1) Kaneko, T.; Yunoki, S.; Millis, A. J. Charge stiffness and long-range correlation in the optically induced η -pairing state of the one-dimensional Hubbard model. *Physical Review Research* **2020**, *2*, 032027.
- (2) Cevolani, L.; Despres, J.; Carleo, G.; Tagliacozzo, L.; Sanchez-Palencia, L. Universal

- scaling laws for correlation spreading in quantum systems with short-and long-range interactions. *Physical Review B* **2018**, *98*, 024302.
- (3) Han, Q.; Millis, A. Lattice energetics and correlation-driven metal-insulator transitions: The case of Ca_2RuO_4 . *Physical Review Letters* **2018**, *121*, 067601.
- (4) Keshavarz, S.; Schött, J.; Millis, A. J.; Kvashnin, Y. O. Electronic structure, magnetism, and exchange integrals in transition-metal oxides: Role of the spin polarization of the functional in DFT+ U calculations. *Physical Review B* **2018**, *97*, 184404.
- (5) Knizia, G.; Chan, G. K.-L. Density matrix embedding: A simple alternative to dynamical mean-field theory. *Physical review letters* **2012**, *109*, 186404.
- (6) Lee, S. J.; Welborn, M.; Manby, F. R.; Miller III, T. F. Projection-based wavefunction-in-DFT embedding. *Accounts of chemical research* **2019**, *52*, 1359–1368.
- (7) Bulik, I. W.; Scuseria, G. E.; Dukelsky, J. Density matrix embedding from broken symmetry lattice mean fields. *Physical Review B* **2014**, *89*, 035140.
- (8) Bulik, I. W.; Chen, W.; Scuseria, G. E. Electron correlation in solids via density embedding theory. *The Journal of chemical physics* **2014**, *141*, 054113.
- (9) Klüner, T.; Govind, N.; Wang, Y. A.; Carter, E. A. Periodic density functional embedding theory for complete active space self-consistent field and configuration interaction calculations: Ground and excited states. *The Journal of chemical physics* **2002**, *116*, 42–54.
- (10) Sharifzadeh, S.; Huang, P.; Carter, E. Embedded configuration interaction description of CO on Cu (111): Resolution of the site preference conundrum. *The Journal of Physical Chemistry C* **2008**, *112*, 4649–4657.
- (11) Libisch, F.; Huang, C.; Carter, E. A. Embedded correlated wavefunction schemes: Theory and applications. *Accounts of chemical research* **2014**, *47*, 2768–2775.

- (12) Gavnholt, J.; Olsen, T.; Englund, M.; Schiøtz, J. Δ self-consistent field method to obtain potential energy surfaces of excited molecules on surfaces. *Physical Review B* **2008**, *78*, 075441.
- (13) Bünermann, O.; Jiang, H.; Dorenkamp, Y.; Kandratsenka, A.; Janke, S. M.; Auerbach, D. J.; Wodtke, A. M. Electron-hole pair excitation determines the mechanism of hydrogen atom adsorption. *Science* **2015**, *350*, 1346–1349.
- (14) Morin, M.; Levinos, N.; Harris, A. Vibrational energy transfer of CO/Cu (100): Nonadiabatic vibration/electron coupling. *The Journal of Chemical Physics* **1992**, *96*, 3950–3956.
- (15) Huang, Y.; Rettner, C. T.; Auerbach, D. J.; Wodtke, A. M. Vibrational promotion of electron transfer. *Science* **2000**, *290*, 111–114.
- (16) Raghavachari, K.; Trucks, G. W.; Pople, J. A.; Head-Gordon, M. A fifth-order perturbation comparison of electron correlation theories. *Chemical Physics Letters* **1989**, *157*, 479–483.
- (17) Andersson, K.; AA, P. P.-. Malmqvist, BO Roos, AJ Sadlej, K. Wolinski. *J. Phys. Chem* **1990**, *94*, 5483.
- (18) Andersson, K.; Malmqvist, P.-Å.; Roos, B. O. Second-order perturbation theory with a complete active space self-consistent field reference function. *The Journal of chemical physics* **1992**, *96*, 1218–1226.
- (19) Bruna, P.; Peyerimhoff, S. Excited-state potentials. *Ab initio methods in quantum chemistry, I* **1987**, 1–98.
- (20) Sherrill, C. D.; Schaefer III, H. F. *Advances in quantum chemistry*; Elsevier, 1999; Vol. 34; pp 143–269.

- (21) Sherrill, C. D. *Computational algorithms for large-scale full and multi-reference configuration interaction wavefunctions*; University of Georgia, 1996.
- (22) Anderson, P. W. Localized magnetic states in metals. *Physical Review* **1961**, *124*, 41.
- (23) Bulla, R.; Costi, T. A.; Pruschke, T. Numerical renormalization group method for quantum impurity systems. *Reviews of Modern Physics* **2008**, *80*, 395.
- (24) Fu, W.; Sachdev, S. Numerical study of fermion and boson models with infinite-range random interactions. *Physical Review B* **2016**, *94*, 035135.
- (25) Gull, E.; Millis, A. J.; Lichtenstein, A. I.; Rubtsov, A. N.; Troyer, M.; Werner, P. Continuous-time Monte Carlo methods for quantum impurity models. *Reviews of Modern Physics* **2011**, *83*, 349.
- (26) Georges, A.; Kotliar, G.; Krauth, W.; Rozenberg, M. J. Dynamical mean-field theory of strongly correlated fermion systems and the limit of infinite dimensions. *Reviews of Modern Physics* **1996**, *68*, 13.
- (27) Kaduk, B.; Kowalczyk, T.; Van Voorhis, T. Constrained density functional theory. *Chemical Reviews* **2012**, *112*, 321–370.
- (28) Ma, H.; Wang, W.; Kim, S.; Cheng, M.-H.; Govoni, M.; Galli, G. PyCDFT: A Python package for constrained density functional theory. *Journal of Computational Chemistry* **2020**,
- (29) Souza, A.; Rungger, I.; Pemmaraju, C.; Schwingenschlögl, U.; Sanvito, S. Constrained-DFT method for accurate energy-level alignment of metal/molecule interfaces. *Physical Review B* **2013**, *88*, 165112.
- (30) Behler, J.; Delley, B.; Reuter, K.; Scheffler, M. Nonadiabatic potential-energy surfaces by constrained density-functional theory. *Physical Review B* **2007**, *75*, 115409.

- (31) Mavros, M. G.; Van Voorhis, T. Communication: CDFT-CI couplings can be unreliable when there is fractional charge transfer. *The Journal of Chemical Physics* **2015**, *143*, 231102.
- (32) Jin, Z.; Dou, W.; Subotnik, J. E. Configuration interaction approaches for solving quantum impurity models. *The Journal of Chemical Physics* **2020**, *152*, 064105.
- (33) Chen, J.; Jin, Z.; Dou, W.; Subotnik, J. Electronic Structure for Multielectronic Molecules near a Metal Surface. *The Journal of Physical Chemistry C* **2021**, *125*, 2884–2899.
- (34) Wu, Q.; Van Voorhis, T. Direct optimization method to study constrained systems within density-functional theory. *Physical Review A* **2005**, *72*, 024502.
- (35) Wright, S.; Nocedal, J., et al. Numerical optimization. *Springer Science* **1999**, *35*, 7.
- (36) Filatov, M.; Shaik, S. A spin-restricted ensemble-referenced Kohn–Sham method and its application to diradicaloid situations. *Chemical physics letters* **1999**, *304*, 429–437.
- (37) Kowalczyk, T.; Tsuchimochi, T.; Chen, P.-T.; Top, L.; Van Voorhis, T. Excitation energies and Stokes shifts from a restricted open-shell Kohn-Sham approach. *The Journal of chemical physics* **2013**, *138*, 164101.
- (38) Alguire, E.; Subotnik, J. E. Diabatic couplings for charge recombination via Boys localization and spin-flip configuration interaction singles. *The Journal of Chemical Physics* **2011**, *135*, 044114.
- (39) Krylov, A. I. Spin-flip configuration interaction: an electronic structure model that is both variational and size-consistent. *Chemical Physics Letters* **2001**, *350*, 522–530.
- (40) Shao, Y.; Head-Gordon, M.; Krylov, A. I. The spin-flip approach within time-dependent density functional theory: Theory and applications to diradicals. *The Journal of chemical physics* **2003**, *118*, 4807–4818.

- (41) Zhang, X.; Herbert, J. M. Spin-flip, tensor equation-of-motion configuration interaction with a density-functional correction: A spin-complete method for exploring excited-state potential energy surfaces. *The Journal of chemical physics* **2015**, *143*, 234107.
- (42) Casanova, D.; Head-Gordon, M. The spin-flip extended single excitation configuration interaction method. *The Journal of chemical physics* **2008**, *129*, 064104.
- (43) Hiscock, H. G.; Thom, A. J. Holomorphic Hartree–Fock theory and configuration interaction. *Journal of Chemical Theory and Computation* **2014**, *10*, 4795–4800.
- (44) Burton, H. G.; Thom, A. J. Holomorphic Hartree–Fock theory: an inherently multireference approach. *Journal of chemical theory and computation* **2016**, *12*, 167–173.
- (45) Levine, B. G.; Durden, A. S.; Esch, M. P.; Liang, F.; Shu, Y. CAS without SCF—Why to use CASCI and where to get the orbitals. *The Journal of Chemical Physics* **2021**, *154*, 090902.

Graphical TOC Entry

Some journals require a graphical entry for the Table of Contents. This should be laid out “print ready” so that the sizing of the text is correct.

Inside the tocentry environment, the font used is Helvetica 8 pt, as required by *Journal of the American Chemical Society*.

The surrounding frame is 9 cm by 3.5 cm, which is the maximum permitted for *Journal of the American Chemical Society* graphical table of content entries. The box will not resize if the content is too big: instead it will overflow the edge of the box.

This box and the associated title will always be printed on a separate page at the end of the document.